Chemistry
A European
Journal

Chemistry
Europe
European Chemical
Societies Publishing

Reprint

WILEY-VCH

Chemistry–A European Journal
Review
doi.org/10.1002/chem.202100007
Chemistry Europe
European Chemical Societies Publishing

Sensors

Overview of N-Rich Antennae Investigated in Lanthanide-Based Temperature Sensing

Flore Vanden Bussche,[a, b] Anna M. Kaczmarek,[b] Veronique Van Speybroeck,[c] Pascal Van Der Voort,[b] and Christian V. Stevens*[a]

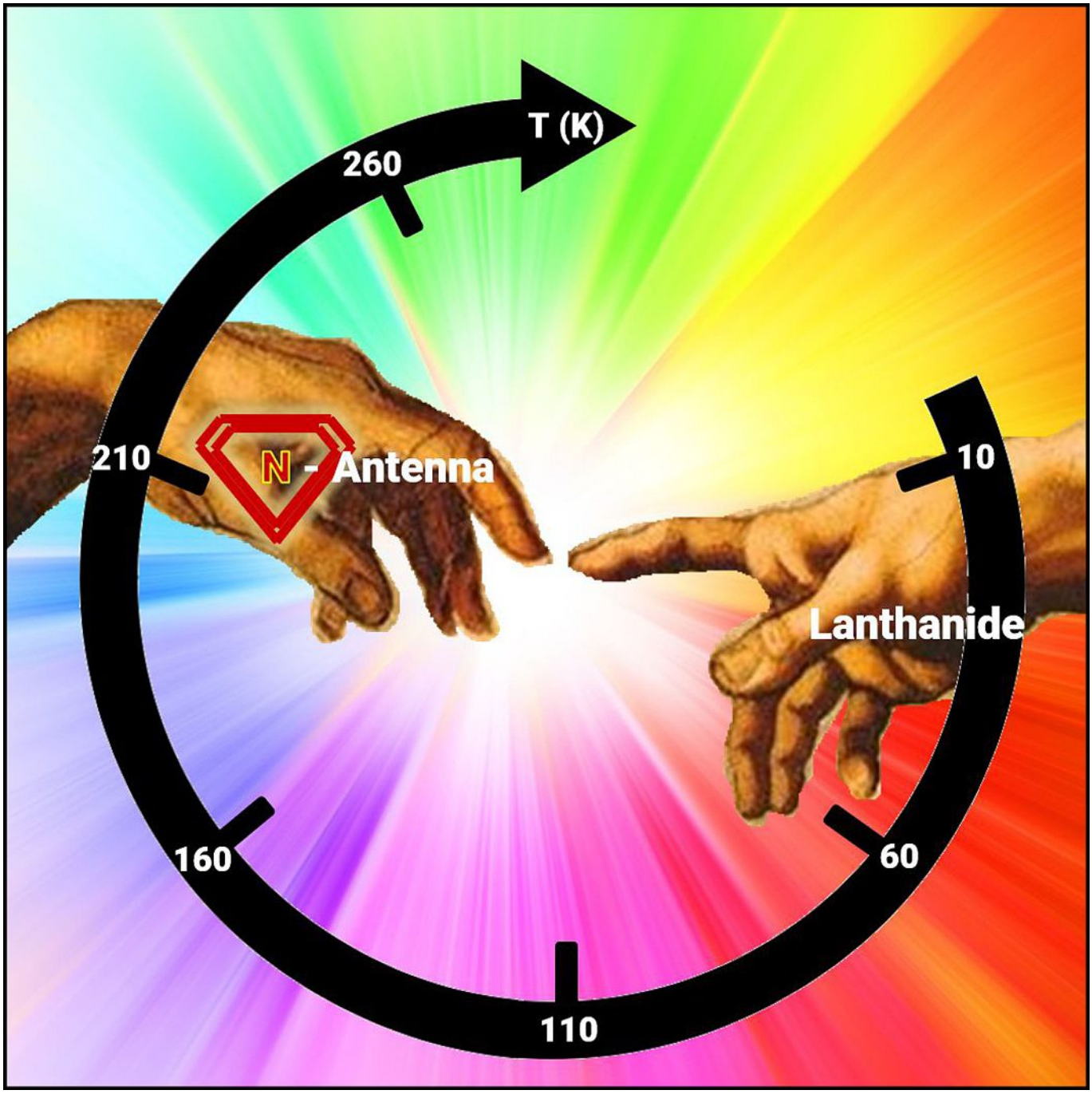

Abstract: The market share of noncontact temperature sensors is expending due to fast technological and medical evolutions. In the wide variety of noncontact sensors, lanthanide-based temperature sensors stand out. They benefit from high photostability, relatively long decay times and high quantum yields. To circumvent their low molar light absorption, the incorporation of a light-harvesting antenna is required. This Review provides an overview of the nitrogen-rich antennae in lanthanide-based temperature sensors, emitting in the visible light spectrum, and discusses their temperature sensor ability. The N-rich ligands are incorporated in many different platforms. The investigation of different antennae is required to develop temperature sensors with diverse optical properties and to create a diverse offer for the multiple application fields. Molecular probes, consisting of small molecules, are first discussed. Furthermore, the thermometer properties of ratiometric temperature sensors, based on di- and polynuclear complexes, metal–organic frameworks, periodic mesoporous organosilicas and porous organic polymers, are summarized. The antenna mainly determines the application potential of the ratiometric thermometer. It can be observed that molecular probes are operational in the broad physiological range, metal–organic frameworks are generally very useful in the cryogenic region, periodic mesoporous organosilica show temperature dependency in the physiological range, and porous organic polymers are operative in the cryogenic-to-medium temperature range.

Introduction

The history of temperature sensing goes back to the Renaissance. From then on, measuring the temperature has challenged many great minds, from Galileo Galilei to Daniel Gabriel Fahrenheit and Andres Celsius.[1] Temperature affects nearly all biological and engineered systems.[2] Thermometers are therefore required in countless scientific and industrial environments, such as chemicals, oil and gas, consumer electronics, energy and power, automotive, healthcare, food and beverages, metals and mining, aerospace and defense, glass, and pulp and paper.[3–7] Their market share is depicted in Figure 1.[8] The temperature sensor market is expected to grow from USD 6.3 billion in 2020 to USD 8.8 billion by 2027, as recently projected in a market analysis by Markets and Markets.[8] Thermometers are subdivided into different categories. A distinction is based on the level of contact between sample and sensor; invasive sensors are in direct contact with the sample and non-invasive sensors measure the temperature remotely.[9] This Review focuses on the latter, since their growth potential is tremendous, based on the current device miniaturization, fast technological developments and advanced healthcare equipment.[8] In these domains, contact is impossible due to the scale of the sample, fast movement or inaccessibility of the object. Temperature gradients are visualized in for example photonic devices, microfluidics, micro-electronics, catalytic processes, and internal parts of combustion engines.[10–15] The application potential in the medicinal fields covers for instance in vivo thermal imaging and early tumor detection.[16–21] Current noncontact techniques are for example infrared thermography, thermoreflectance and thermographic phosphor luminescence. The infrared temperature sensors and fiber-optic temperature sensors are currently the main industrial applied non-contact thermometers. The thermographic phosphor luminescence is the upcoming and most promising accurate technique and is based on the thermal reading through phosphor light emission. Luminescent thermal sensors are derived from for example, organic dyes, ruthenium complexes, polymers, quantum dots (QDs) and materials doped with lanthanide ions. The QDs and materials doped with lanthanide ions benefit from higher photostability. Since QDs generally include highly toxic elements (e.g. Cd), the main focus involves lanthanide-based materials showing temperature dependent luminescence.[9,22–25] Different platforms are used in the design of lanthanide-based materials, such as metal organic frameworks, inorganic materials (phosphors and nanocrystals), inorganic–organic materials (coordination polymers, mesoporous silica).

[a] *F. Vanden Bussche, Prof. Dr. C. V. Stevens*
Department of Green Chemistry and Technology
Ghent University
Ghent (Belgium)
E-mail: Chris.Stevens@ugent.be

[b] *F. Vanden Bussche, Prof. Dr. A. M. Kaczmarek, Prof. Dr. P. Van Der Voort*
Department of Chemistry
Ghent University
Krijgslaan 281 (S3), 9000, Ghent (Belgium)

[c] *Prof. Dr. V. Van Speybroeck*
Department of Applied Physics
Ghent University
Technologiepark 46, 9052, Zwijnaarde (Belgium)

The ORCID identification number(s) for the author(s) of this article can be found under:
https://doi.org/10.1002/chem.202100007.

The Importance of Lanthanides

Trivalent lanthanide ions (Ln^{3+}) absorb and emit electromagnetic radiation in the entire electromagnetic spectrum.[26,27] These ions are stable and narrow band emitters. The remarkable optical properties of lanthanide ions arise from partial filling of their 4f orbitals.[28–30] The electrons in this orbital are shielded by the filled 5s and 5p orbitals, since these appear further from the nucleus than the 4f orbital. Therefore, they do not overlap with ligand orbitals. The shielding implies spectroscopic and magnetic properties that are largely unaffected by the environment. The luminescence of trivalent lanthanides arises from 4f–4f transitions, and since these are shielded, the emission bands are narrow and well defined. Moreover, lanthanide ions have relatively long decay times, high quantum

yields and high photostability. The 4f–4f transitions are however principally forbidden, resulting in inefficient excitation of the Ln^{3+} ion and thus low absorption coefficients. To circumvent this drawback, organic ligands, which have allowed absorption transitions, are incorporated as antennae to capture the energy and transfer it to the lanthanides. This principle is known as "the antenna effect" and is illustrated in Figure 2.[31]

In this process, first the ligand absorbs energy and undergoes transition from its singlet ground state S_0 to an excited S_1 state; secondly, the singlet S_1 state can transfer energy to the triplet T_1 state, via intersystem crossing (ISC). Thirdly, the energy from the ligand is transferred to the lanthanide excited states, known as energy transfer. Lastly (and in the ideal scenario), radiative (light) emission occurs as the luminescent energy level relaxes back to lower lying (ground) state. The larger the energy gap between the lanthanide's emitting level and its highest lower lying energy level, the more intense luminescence will be. Furthermore, in order to have efficient energy transfer from the triplet state to the lanthanide ion, the energy of the triplet level should be closely matched with the Ln^{3+} accepting levels. The energy difference between T_1 of the ligand and the energy state of the lanthanide should therefore be about 2000–4000 cm^{-1}.[32] The temperature dependent luminescence originates from the balance between three possible pathways: 1) thermal relaxation (vibrational relaxation of lanthanide ions), 2) energy transfer, related to the energy levels, 3) energy back transfer from the lanthanide ion to the excited triplet state of the ligand (enhanced when their energy gap is less than 1850 cm^{-1}).[32–35] In the design of the lanthanide complex, selection of the lanthanide and the appropriate antennae is therefore crucial. Another incentive for the selection of the antenna is the creation of a Lewis adduct.[36,37] The trivalent lanthanide ions are hard Lewis acids, the lanthanide complex will therefore preferentially interact with at least one Lewis base. N-Donor ligands phenanthroline and bipyridine are popular bases since the resulting complex often shows intense luminescence. As an example, the luminescence and the emission spectra of [Eu_x, Tb_{1-x}](L)-bdc are shown in Figure 3.[38]

Moreover, the extra Lewis base minimizes radiationless deactivation.[39] Furthermore, electronegative donor atoms are preferred in the trivalent lanthanide complex, with O-donors yield-

Flore Vanden Bussche graduated in 2016 as Bioengineer—Chemistry and Bioprocess technology at Ghent University. She is affiliated to the research groups SynBioC (Synthesis, Bioresources and Bioorganic Chemistry) and COMOC (Center for Ordered Materials, Organometallics and Catalysis). Her research career started during her master thesis, with a focus on the synthesis of powerful and selective Histone Deacetylase Inhibitors. During her PhD, she specialized in the field of porous polymers (POPs, CTFs, COFs) for photo-applications. A highlight in her PhD career was the research stay in the group of Prof. Bettina Lotsch at the Max Planck Institute for Solid State Research in Stuttgart.

Anna M. Kaczmarek is a materials chemist studying luminescent nanothermometers and their applications in various fields. She develops nanomaterials mostly based on lanthanide ions. Anna M. Kaczmarek received her master degree in chemistry in Poznan, Poland. In 2015, she defended her PhD in Chemistry at Ghent University, Belgium. She carried out postdoctoral research in three different groups at Ghent University and also carried out several long stays abroad at Cordoba University, Spain, and Utrecht University, Netherlands. In 2020 she obtained a permanent position at the Department of Chemistry of Ghent University (Belgium) and started the NanoSensing group, which will study nano-sized optical sensors and specialize in nanothermometry. She recently obtained a prestigious ERC Starting Grant on the topic of thermometry for theranostic applications.

Veronique Van Speybroeck is full professor at Ghent University and head of the Center for Molecular modeling (http://molmod.ugent.be). She obtained her PhD in 2001 from Ghent University. She is recipient of two flagship grants from the European Research Council: a Starting and Consolidator grant. Her expertise lies in first principle kinetics and molecular dynamics simulations of complex chemical transformations in nanoporous materials. She is also an elected member of the Royal (Flemish) Academy for Science and the Arts of Belgium.

Pascal Van Der Voort is a full professor at Ghent University and the director of the Center for Ordered Materials, Organometallics and Catalysis (COMOC). His research focuses on the development of novel (hybrid) ordered porous materials, including PMOs, MOFs, COFs and CTFs. Application fields of these materials are heterogeneous catalysis, sorption, gas separation, luminescence, sensing photocatalysis and electrocatalysis.

Prof. Dr. ir. Christian V. Stevens (1965) is senior full professor at the Department of Green Chemistry and Technology at the Faculty of Bioscience Engineering (Ghent University, Belgium). He graduated in 1988 and obtained a PhD in 1992 at Ghent University. He then performed postdoctoral work at the University of Florida guided by Prof. Alan Katritzky in 1992–1993 as a NATO Research Fellow. In 2014, he became senior full professor. Chris has published over 310 international peer reviewed papers and 20 patents and received several prizes. His research interest focuses on synthetic heterocyclic chemistry, the use of flow chemistry and the use of renewable resources for the industry. He is an active member of the American Chemical Society and Fellow of the Royal Society of Chemistry Britain.

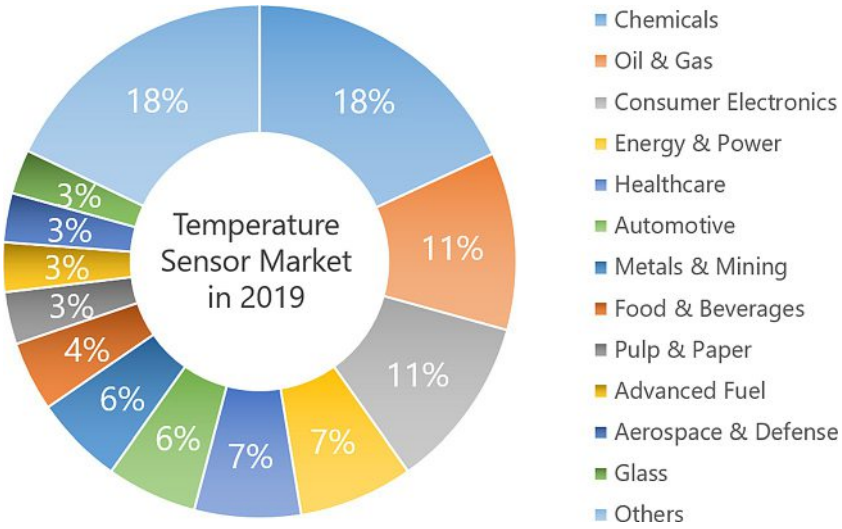

Figure 1. Overview of end-user industries for the temperature sensor market in 2019, valued at USD 6,043 million. 'Others' include HVAC, water & wastewater management, cement, telecommunications and agriculture. Figure adapted from Ref. [8].

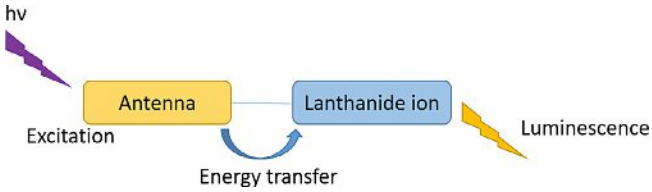

Figure 2. Simplified illustration of lanthanide-based luminescence.

ing the most effective coordination properties towards lanthanides. When looking at the literature, lanthanide β-diketonate complexes are the most popular, forming mostly 'tris' complexes with two coordination sites available for the neutral Lewis base ligand. Europium and terbium are the most widely studied luminescent lanthanide ions, since their energy level matches well with the triplet level of the reported N-rich ligands which feature intense luminescence, followed by dysprosium and samarium. These trivalent ions show emission in the visible light spectrum, however, near-infrared (NIR) emission is also observed. This Review provides an overview of the *N*-donor antennae used in temperature sensing, consisting of these particular lanthanide ions, with the focus on resulting luminescent emission in the visible light spectrum. N-rich ligands have been incorporated in multiple platforms containing antennae ligands, ranging from porous materials as metal organic frameworks (MOFs), covalent organic frameworks (COFs), porous organic polymers (POPs) and periodic mesoporous organosilica (PMOs) over nonporous coordination polymers,

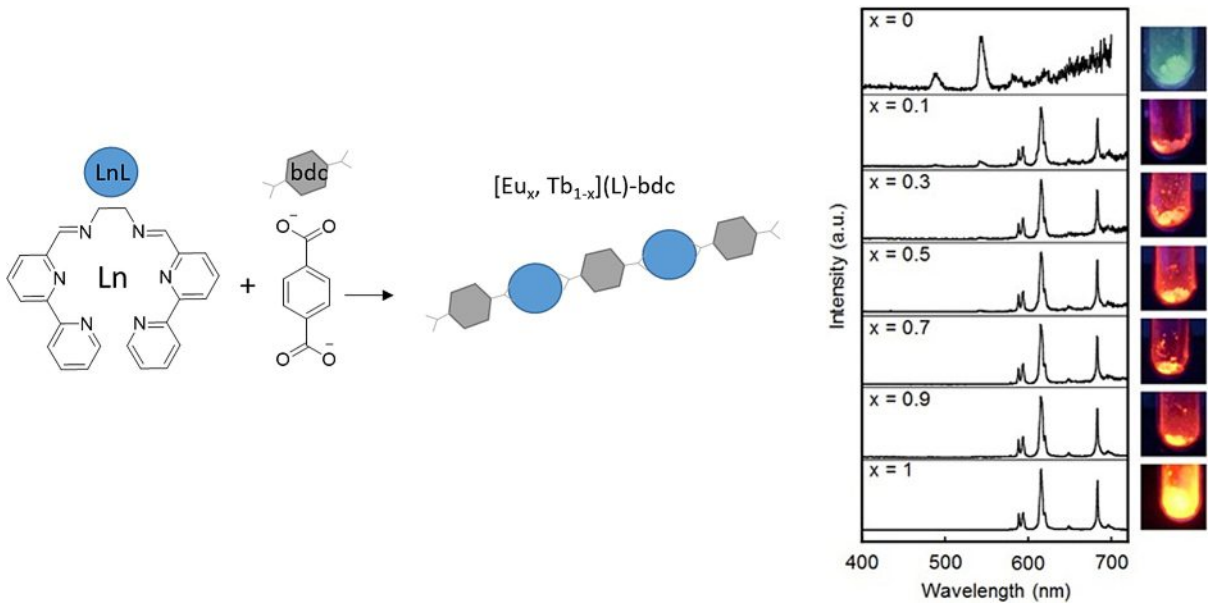

Figure 3. The emission spectra of [Eu$_x$, Tb$_{1-x}$](L)-bdc in the solid state at room temperature (excited at 315 nm), and the corresponding photographs of each solid sample showing the luminescence.[38] Reprinted with permission from Ref. [38]. Copyright 2014, Springer Nature.

small molecules and organic–inorganic hybrids.[23,32,39–47] The investigation of different antennae is required to develop temperature sensors with divers optical properties and to create a divers offer for the different application fields. Sensors are typically operative in a distinct temperature region, namely cryogenic (up to 100 K), medium (100–300 K), biological/physiological (298–323 K) and the high temperature region ($\geq$450 K). This Review provides an overview of the nitrogen-rich antennae used in the different material categories and discusses their corresponding temperature sensor ability. Previous reported reviews mostly focus on one category of material, thereby covering for example the MOFs, PMOs or small molecules.[32,42–44,47,48] With this Review, we show that the base in the design of every temperature sensor is equal throughout all types of material, covering the conscious choice of the N-donor antennae and lanthanide ions when having the ultimate goal in mind. In the first part, lanthanide-based temperature sensors with N-rich antennae in small molecules will be discussed. These complexes merely depend on the emission intensity of a single transition, creating a system which can be affected by fluctuations of the measurement equipment. To avoid these fluctuations, sensors based on two transitions, known as ratiometric temperature sensors, were developed. In the discussion of the ratiometric thermometers, a distinction is made between the following types of materials; di- and polynuclear complexes, metal–organic frameworks, periodic mesoporous organosilicas, and porous organic polymers.

Important Performance Parameters for Temperature Sensors

The performance of different lanthanide-based temperature sensors is assessed on five key parameters. These parameters are crucial for a quantitative comparison and evaluation of the developed thermometers. An in-depth review on these different parameters is recently conducted by Carlos and co-workers.[9] Here, we briefly summarize their most important features. The first parameter is the relative thermal sensitivity (S_r), indicating the relative change of the thermometric parameter Δ [Eq. (1)] per degree of temperature change (Equation (2), % K^{-1}; S_r = relative thermal sensitivity). This valuable parameter is independent of the nature of the thermometer, allowing direct comparison of ratiometric thermometers over different categories of materials. The maximum value of S_r, S_m, at a certain temperature T_m is mostly reported. The second parameter is the temperature uncertainty (δT), also known as temperature resolution. It describes the smallest temperature change resolvable by the thermometer [Eq. (3)]. This parameter depends on both the material and the experimental setup (f. ex. acquisition conditions, experimental detection setup, signal-to-noise ratio). The third parameter is the repeatability R, illustrating the ability of the thermometer to repeatedly provide the same result, under the same circumstances [Eq. (4)]. The fourth and fifth parameters are resolution and reproducibility. The spatial δx and temporal δt resolutions are, respectively the minimum resolvable distance or time interval between two measurements. The reproducibility is defined as the change of the same measurement, carried out under modified circumstances, such as different equipment, different measurement method, different operator.

$$\Delta = \frac{I1}{I2} \tag{1}$$

with I_1 and I_2 the integrated intensities of two transitions

$$S_r = 100\% \times \left|\frac{1}{\Delta}\frac{\partial\Delta}{\partial T}\right| \tag{2}$$

$$\delta T = \frac{1}{S_r}\frac{\delta\Delta}{\Delta} \tag{3}$$

$$R = 1 - \frac{max|\Delta c - \Delta i|}{\Delta c} \tag{4}$$

with Δc the mean thermometric parameter and Δi the thermometric parameter measured at each temperature.

The temperature will affect the luminescence of the discussed temperature sensors. The induced changes are monitored based on distinct parameters of the emitting center.[23] A distinction is made between 1) the integrated emission intensity of a single transition or a pair of transitions, 2) the spectral shift, polarization, or bandwidth of a certain transition, 3) lifetime measurements, focusing on time-decay intensity profiles of the excited emitting states. As stated before, this Review focuses first on small molecules with a single transition, thereby reporting the luminescence lifetime of the developed temperature sensors. Secondly, the focus is on ratiometric temperature sensors. Here, the measurement is based on the relative change in the intensity ratio of two independent energy-close transitions. The emission bands originate either from a single luminescent center, known as single-center thermometers, or from two distinct emitting centers, known as dual-center thermometers. The dual center thermometers are more discussed in this Review on organic based antennae, as dual type thermometers are more common in such materials. In inorganic nanoparticles, single center thermometers, for example, Nd^{3+} and Er^{3+}, are very common.[6]

N-Rich Antennae Incorporated in Small Molecules

The first group of compounds that will be discussed are the small molecule emissive probes. In these probes, one trivalent lanthanide ion is incorporated in the structure. The temperature sensors are characterized based on their luminescence lifetime τ, defined as the average time a molecule stays in the excited state.[49] This is calculated as the inverse of the sum of constants of radiative (k_r) and nonradiative (k_{nr}) processes [Eq. (5)].

$$\tau = \frac{1}{(k_r + k_{nr})} \tag{5}$$

In 2003, Dalton et al. synthesized a temperature sensitive paint, based on a tris(β-diketonate) phenanthroline europ-

ium(III) complex **1**.[50] The material showed temperature dependence over the temperature range 278 to 318 K, when dissolved in a polymer matrix. In the same year, Amao et al. incorporated tris(4,4,4-trifluoro-1-(2-thienyl)-1,3-butanediono)-1,10-phenanthroline europium(III) ($Eu(TTA)_3Phen$) **2** into poly(*N*-dodecylacrylamide) (PDDA) film, thereby creating a temperature sensitive sensor in the range of 320–370 K.[51] In 2004, Dalton et al. incorporated complex **5** and **6** in a 1/600 dilution in fluoroacrylic polymer (FIB), creating a temperature sensitive paint in the temperature region 278–323 K.[39] In 2006, Wolfbeis et al. developed three complexes **3**, including the dipyrazolyltriazine tris(β-diketonate) europium(III) complex **3a** ($Eu(TTA)_3(dpbt)$).[49] The dipyrazolyltriazine antenna allowed absorption in the visible light spectrum. Upon excitation at the ligand charge-transfer band (405 nm), their luminescence lifetime drastically decreased with increasing temperature. Furthermore, they dispersed the europium complex onto a poly(vinyl methyl ketone) (PVMK) film to improve the stability, after which temperature dependency was found between 274 K and 333 K. In 2008 and 2010, Stich et al. successfully doped the europium(III) complex **3** into poly(vinyl chloride) (PVC) polymer to develop a temperature-sensitive-paint (TSP).[52,53] The TSP shows temperature dependency from 270 K to 310 K. In 2018 and 2020, Lapaev et al. address the bottleneck of Eu^{3+}-based films: their moderate photostability. They developed more photostable temperature probes by using Eu^{III} β-diketonate complexes **8**, **9** with an anisometric geometry (i.e., the ratio of the long inertial axis of the molecule to its short inertial axis in the ellipsoid of revolution). Through the melt-processing technique, stable vitrified films are established from powders of the complexes. Complexes with longer alkyl chains undergo a glass transition with the formation of a vitrified, transparent, and amorphous film, while shorter alkyl substituents crystallize and decompose upon heating.[54–56] An overview of different Eu^{3+}-containing temperature sensor complexes is given in Table 1. Two possible mechanisms are responsible for the temperature dependent behavior of these europium-based complexes. The first is based on the thermal quenching process (nonradiative) from excited Eu^{III} to vibrational relaxation.[57,58] The energy gap between the emitting level and the highest accepting level in 4f–4f transition of Eu^{3+} ions ($^5D_0$–$^7F_6$: 12297 cm^{-1}) is well-matched with the overtone of C–H and O–H vibrational frequencies, as depicted in Figure 4.[32] The coordination of water or other solvent molecules therefore potentially quenches the luminescence of the lanthanide ions. In a second mechanism, low-lying ligand-to-metal charge transfer states are responsible for the quenching of the thermal luminescence of Eu^{3+} ions.[59] Overall, the europium-based probes are photoexcited in the 350–450 nm range and all probes are operational in the physiological temperature range.

Table 1. Overview of the different N-rich antenna used in small molecule based temperature probes.

Complex/Matrix	Temperature range [K]	Luminescence lifetime τ range [μs]	Ref.
1/PMMA	278–318	340–150	[50]
2/PDDA	320–370	N.D.[a]	[51]
3a/PVMK	274–333	500–190	[49]
3b/PVMK	274–333	455–150	[49]
3c/PVMK	274–333	625–240	[49]
3a/PVC	270–310	550–320	[53]
4/ PVDC-co-AN	278–328	N.D.[a]	[62]
5/FIB	278–323	350–80	[39]
6/FIB	278–323	400–110	[39]
7/PMMA	323–333	N.D.[a]	[63]
8/None	298–348	537–210	[55]
9/None	270–370	561–37	[54]
10/None	143–253	373–33	[60]
11(Tb)/None	18–320	730–829	[61]
11(Dy)/None	18–320	16–18	[61]

PMMA: poly(methyl methacrylate), PDDA: poly(*N*-dodecylacrylamide), PVMK: poly(vinyl methyl ketone), PVC: poly(vinyl chloride), PVDC-co-AN: poly (vinylidene chlorideco-acrylonitrile), FIB: fluoroacrylic polymer. [a] The reported temperature dependency is based on temperature intensity.

Next to europium, terbium-based small molecules are designed as temperature sensor. The energy gap of Tb^{III} ion ($^5D_4$–$^7F_0$: 14800 cm^{-1}) is larger than the energy gap of Eu^{III} ions, the thermal quenching is therefore suppressed and temperature dependence is mainly determined by energy back transfer from the excited Tb^{III} ions to the excited triplet state of the antenna.[32] Energy back transfer is enhanced if this energy gap is less than 1850 cm^{-1}.[34] An example of a terbium containing

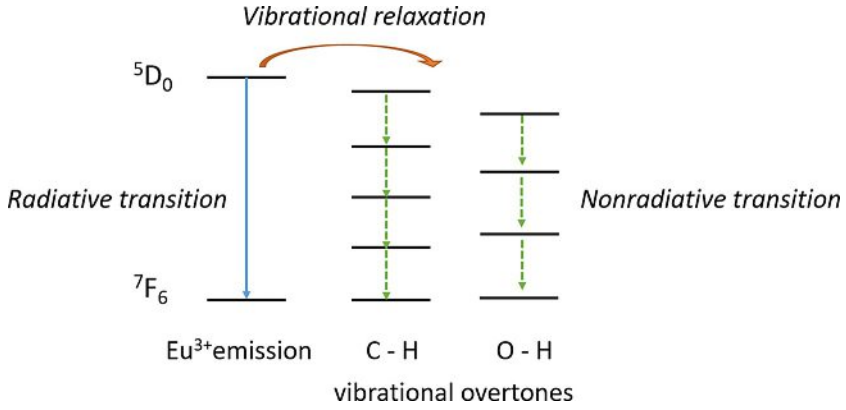

Figure 4. The vibrational overtones of C–H and O–H match the energy gap of the Eu^{III} ion.

small molecule is developed by Lapaev et al. in 2018.[60] The phenanthroline tris(1-(4-(4-propylcyclohexyl)-phenyl)decane-1,3-dionate (cpdk) Tb^{III} complex ($Tb(cpdk)_3(phen)$) **8** shows temperature dependency in the region 143–253 K, after designing a film of the complex via a melt-processing technique. Furthermore, Brusso and co-workers coordinated the ligand 2-amidinopyridine (PyAm) to terbium and dysprosium ($Ln(acac)_3(PyAm)$).[61] The complexes show temperature-dependent changes in the thermal distribution of the Stark sublevels, showing different thermal populations within the same transition. At the supramolecular level, neighboring mononuclear molecules interact through hydrogen bonding (illustrated in Figure 5). For the terbium complex, the lifetime value increased from 730 μs at 12.7 K to 829 μs at 320 K. For the dysprosium complex, the lifetime was reached at the detection limit of the equipment, which may impact the accuracy. An in-

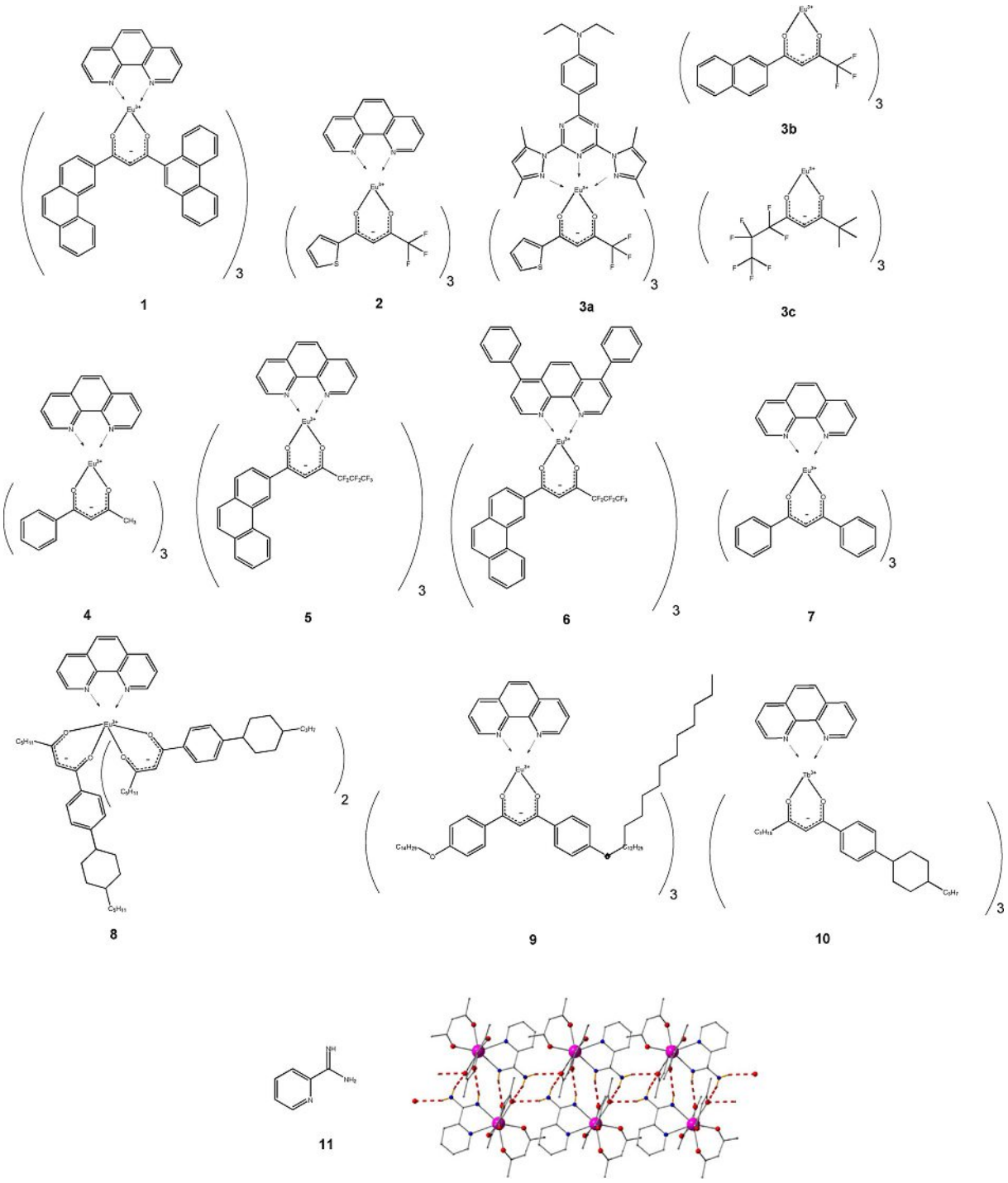

Figure 5. Overview of the Eu^{3+} and Tb^{3+} complexes with nitrogen-rich antennae used in small-molecule-based temperature sensors. (Reprinted with permission from Ref. [61], Copyright 2020 American Chemical Society)

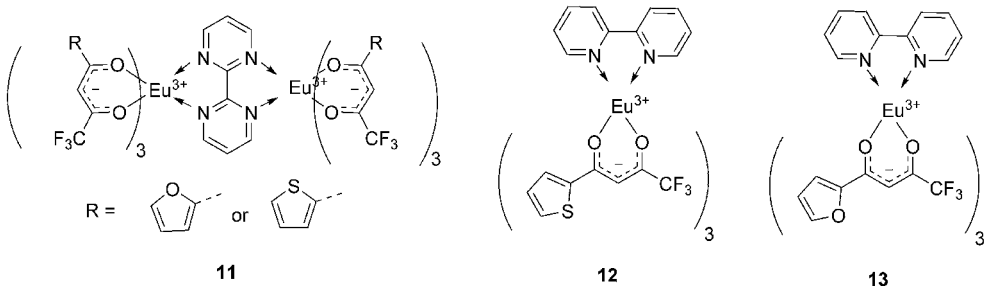

Figure 6. The temperature sensors developed by Swavey and co-workers.[64]

crease in lifetime was reported from 16.25 μs at 12.7 K to 18 μs at 320 K. The triplet level of PyAm was determined to be 26500 cm^{-1}, thereby promoting efficient ligand to metal energy transfer. This was the first report experiencing such behavior over a wide temperature range. The authors therefore stated further research was required to explain the observed increase in lifetime. Compared to the europium complexes, the terbium complex operates in a lower temperature region.

The discussed small molecule-based temperature sensors are all mononuclear lanthanide complexes. In order to improve energy transfer, polynuclear lanthanide complexes are highly desirable. Swavey and co-workers designed two di-nuclear bipyrimidine Eu^{III} β-diketonate complexes **11** (Figure 6) and suggested electronic communication between the Eu^{3+}-ions via the bipyrimidine bridge, yielding a temperature sensor operative in the range 278–318 K.[64] The comparison of luminescent behavior with the mononuclear bipyridine Eu^{III} β-diketonate complexes **12**, **13** (Figure 6) did however not show any difference, implying little electronic communication. Murugesu and co-workers followed the same synthetic strategy.[65] They created three dinuclear terbium complexes, bridged by a planar 2,2′-bipyrimidine ligand. The remainder of the coordination environment is occupied by beta-diketonate ligands (acetylacetonate (acac), 1,1,1-trifluoroacetylacetonate (tfac), hexafluoroacetylacetone (hfac)). The complex with the acac and the tfac ligands shows temperature dependency in the temperature range 80–260 K, with a decrease in luminescence lifetime of 960–25 μs and 950–100 μs, respectively. The hfac-based complex showed temperature dependency in the 80–323 K, with a decrease in luminescence lifetime from 960-350 μs. The T_1 energy of the ligands are approximately 24800 (acac), 22700 (tfac), 22200 (hfac) and 23350 (bpm) cm^{-1}. The sensitization mechanism therefore depends on an efficient ligand-to-metal energy transfer of all the ligands involved.

N-Rich Antennae Incorporated in Di- and Polynuclear Complexes

The discussed materials all depend on the emission intensity of a single transition, creating a system dependent on illumination fluctuations. The incorporation of different trivalent lanthanide ions allows its use as a ratiometric temperature sensor. A thermometer should therefore ideally have two discriminable emission peaks, in order to observe a clear luminescence and coherent temperature difference. The ratio of the two peaks eliminates fluctuations in 1) the excitation source, 2) the detector, 3) the concentration and inhomogeneity of the luminescent centers in the material. The ratiometric thermometers are subdivided in single center and dual center emissions. In a single center, the ratio arises from the emission transitions of two distinct transitions from the same emitting center, demonstrated in dysprosium-based sensors. However, Dy-based sensors are rare, since it is hard to find materials, which show strong Dy^{3+} luminescence due to the high energy accepting level of Dy^{3+} and the corresponding difficulty to find a matching triplet level. In a dual center, the ratio is calculated based on two different emitting centers, as specified in the introduction. The performance of different ratiometric thermometers in this Review is compared using the following parameters: 1) temperature sensitivity, expressed in units of % change per degree of temperature change (% K^{-1}), 2) temperature uncertainty, 3) repeatability and reproducibility. The temperature sensitivity, repeatability and reproducibility should be as high as possible, while the temperature uncertainty should not exceed 1 K. These different parameters have recently thoroughly been reviewed.[9]

A first example of a ratiometric thermometer is the luminescent organic polyhedra $Eu_{0.4}Tb_{3.6}$(triazole-pyridine-amido **14**)$_4$ developed by Sun and co-workers.[66] This soluble cage-like structure, depicted in Figure 7, shows temperature dependency in the region 200–360 K with a temperature sensitivity of 1.52% K^{-1}. The energy gap between the triplet state of the ligand **14** (22321 cm^{-1}) and the $^5D_4$ energy level of Tb^{3+}-ions (20500 cm^{-1}) is smaller than 1850 cm^{-1}, implying energy back transfer from the excited Tb^{3+} state to the excited triplet state of the ligand. Subsequently, Tanner et al. developed a heterodinuclear Eu/Tb complex (cycEu-phTb **15**) active in the temperature region 10–200 K, with a temperature sensitivity of 1.86% K^{-1}.[67] In 2018, Li and co-workers developed a flexible and transparent film through the solution casting method.[68] They cased a methanol solution of $Eu_{0.5}Tb_{0.5}$L (**16**) with a small amount of dimethylformamide solution of poly(methyl methacrylate) (PMMA), resulting in $Eu_{0.5}Tb_{0.5}$L@PMMA. The film showed temperature dependency in the range 77–297 K with a temperature sensitivity of 0.46% K^{-1}. In 2019, Zhou et al. developed the complex $Tb_{1.95}Eu_{0.05}$pdc **17**, with the ligand pyridine-3,5-dicarboxylic acid (pdc).[69] The material is operative in the physiological range (298–318 K) with a maximum relative

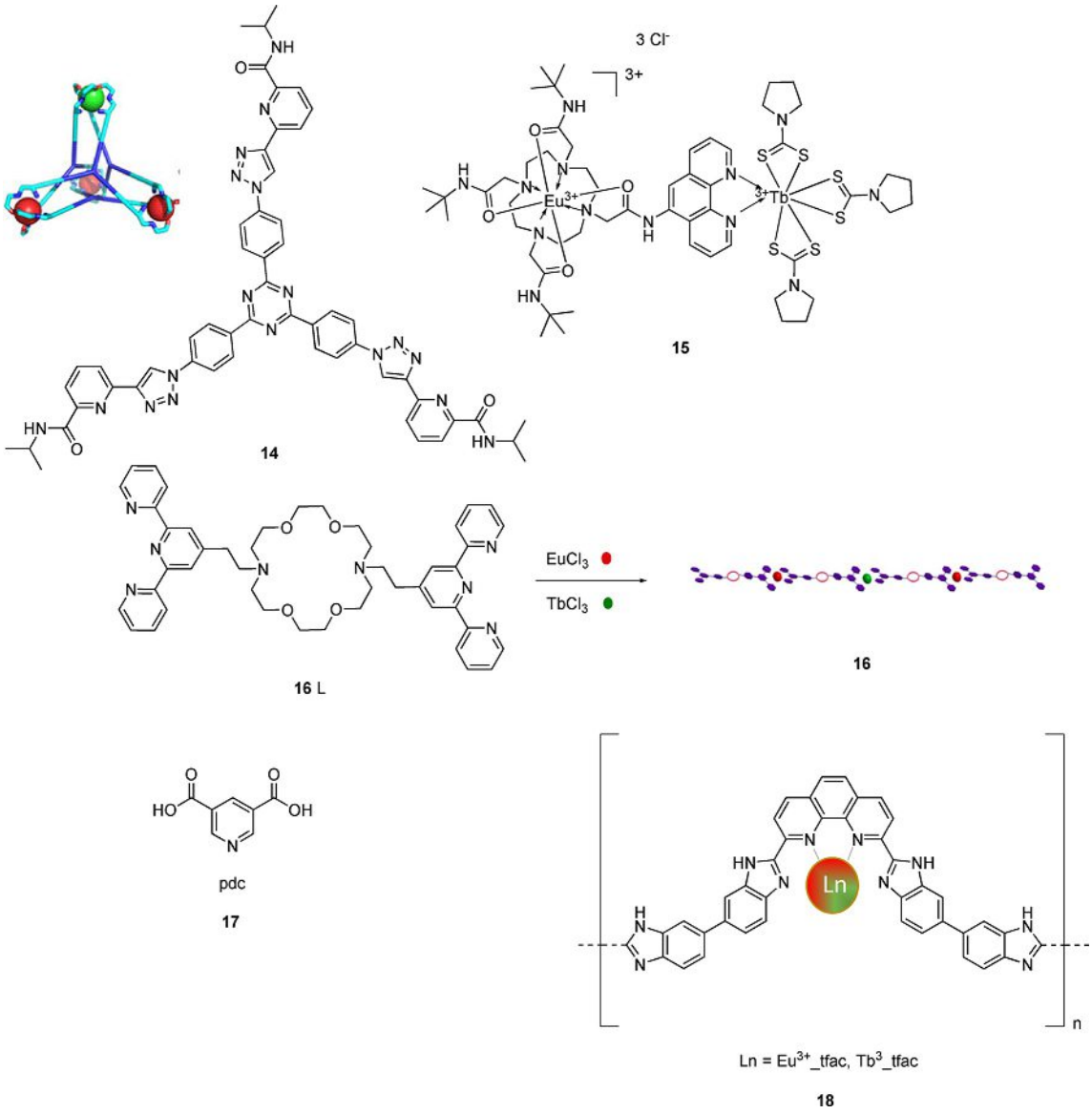

Figure 7. Polyhedra $Eu_{0.4}Tb_{3.6}$(triazole-pyridine-amido **14**)$_4$ developed by Sun and co-workers (image section reproduced from reference [66] with permission. Copyright Wiley-VCH 2018),[66] the dinuclear cycEu-phTb complex **15** of Tanner et al.,[67] $Eu_{0.5}Tb_{0.5}$L (**16**) of Li and co-workers (image section reproduced from Ref. [68] with permission. Copyright 2018 Elsevier)[68] and ligand **17** of the complex $Tb_{1.95}Eu_{0.05}$pdc,[69] and $Tb_{0.5}Eu_{0.5}$_tfac@Phen-polymer **18** of Stevens and Van Der Voort (image section reproduced from Ref. [70] with permission. Copyright 2019 The Royal Society of Chemistry).[70]

sensitivity of 0.64% K^{-1}. The triplet excited state energy is 23 809 cm^{-1} and efficient ligand-to-metal energy transfer (LMET) to the Tb^{3+}-ions and subsequent energy transfer (ET) from Tb^{3+} to Eu^{3+} is observed. In 2019, Stevens and Van Der Voort reported a phenanthroline-based, insoluble polymer ($Tb_{0.5}Eu_{0.5}$_tfac@Phen-polymer **18**).[70] The material showed temperature dependency in the broad physiological range (260–460 K) with a maximum temperature sensitivity of 2.34% K^{-1} at 340 K. The triplet excited state energy of the ligand is 24096 cm^{-1}, the authors therefore assume the transfer of excitation energy from the phen-polymer to the $^5D_4$ accepting level of Tb^{3+} and subsequent transfer to the $^5D_0$ accepting levels of Eu^{3+}. Furthermore, the material showed repeatability up to 98% and good temperature uncertainty ($\delta T < 1$) over the whole studied range.

N-Rich Antennae Incorporated in Metal–organic Frameworks

Metal–organic frameworks (MOFs) and coordination polymers are organic-inorganic hybrid materials with metal ions coordinated to organic ligand linkers. Variation in the metal ions and organic ligands allows the development of endless combinations, resulting in 1D, 2D or 3D structures. Their interesting luminescence properties arise from the metal ions, the ligands, and the interactions between these building units. The creation of dual center emission MOFs proceeds via three routes, and is always based on the measurement of intensities of two transitions of distinct emitting centers (dual center). The first is based on a ligand (the organic linker) and a lanthanide ion, the second on two lanthanide ions (mostly Eu^{3+} and Tb^{3+})

and the third an a dye, hosted in the pores of the MOF, and a lanthanide ion.[41,71] The MOF-based thermometers discussed in this Review all belong to the second category. The presence of multiple luminescent centers creates tunable, ratiometric temperature sensors. The triplet excited state energy level of the organic ligand is ideally located in the range 22000–27000 cm^{-1}, in order to match the main energy accepting levels of Eu^{3+} ($^5D_1$: 19031 cm^{-1}) and Tb^{3+} ($^5D_4$: 20500 cm^{-1}). In 2012, the first Eu^{3+}/Tb^{3+} mixed metal–organic framework was investigated by Cui and co-workers for temperature sensing.[72] The bridging ligand is 2,5-dimethoxy-1,4-benzenedicarboxylate (dmbdc), with a triplet excited state energy of 23306 cm^{-1}. The resulting MOF $Tb_{0.9931}Eu_{0.0069}$dmbdc **19** (Figure 8) showed a maximum temperature sensitivity of 1.15% K^{-1} at 200 K in the region 50–200 K. The incorporation of nitrogen-rich ligands followed rapidly. Higher sensitivities and wider temperature response rates could be achieved by manipulating the energy transfer process, via changing the triplet excited state energy of the organic linker. In a follow-up study by the same research group, the use of the ligand 5-(pyridine-4-yl) isophtalate (pia) **20**, with a higher triplet excited energy (26455 cm^{-1}), resulted in a MOF-based thermometer $Tb_{0.9}Eu_{0.1}$pia with a temperature sensitivity of 3.53% K^{-1} in the region 100–300 K.[73] They assign the increase in sensitivity to the increase in triplet level. However, the ratio of Eu^{3+} and Tb^{3+} present is different in the two samples. Increasing the amount of Tb^{3+} in the MOF, $Tb_{0.99}Eu_{0.01}$pia, resulted in a non-reliable luminescent temperature sensor. The comparison between different MOF-based temperature sensors is therefore complex. Later on, Cui and co-workers developed a MOF, $Tb_{0.957}Eu_{0.043}$cpda, consisting of an organic ligand (5-(4-carboxyphenyl)-2,6-pyridinedicarboxylic acid (cpda) **21**) with a triplet excited state energy of 27027 cm^{-1}. The temperature sensor operates in the region 40–300 K with a maximal sensitivity of 16% K^{-1} (300 K), the wider temperature region and the higher sensitivity are ascribed to the high triplet level of the ligand.[74] Wang and co-workers designed a MOF with the linker 5-(4-(tetrazol-5-yl)phenyl) isophthalic acid (tpi) **22**, $Tb_{0.9122}Eu_{0.0878}$tpi.[75] The material showed temperature dependency in the region 75–250 K with a maximum sensitivity of 4.9% K^{-1} at 250 K. The lanthanide ions are incorporated in the MOF either as metal node through direct synthesis or through post-synthetic functionalization of the organic ligand in the MOF. In 2014, Yan and co-workers investigated the effect of varying the metal node (M) in a mixed M, Ln-MOF. They started from the nanosized MOF In(OH)(bpydc) (bpydc = 2,2′-bipyridine-5,5′-dicarboxylic acid **23**) and incorporated Eu^{3+} and Tb^{3+} via post-functionalization.[76] The bipyridyl moieties serve as free Lewis basic coor-

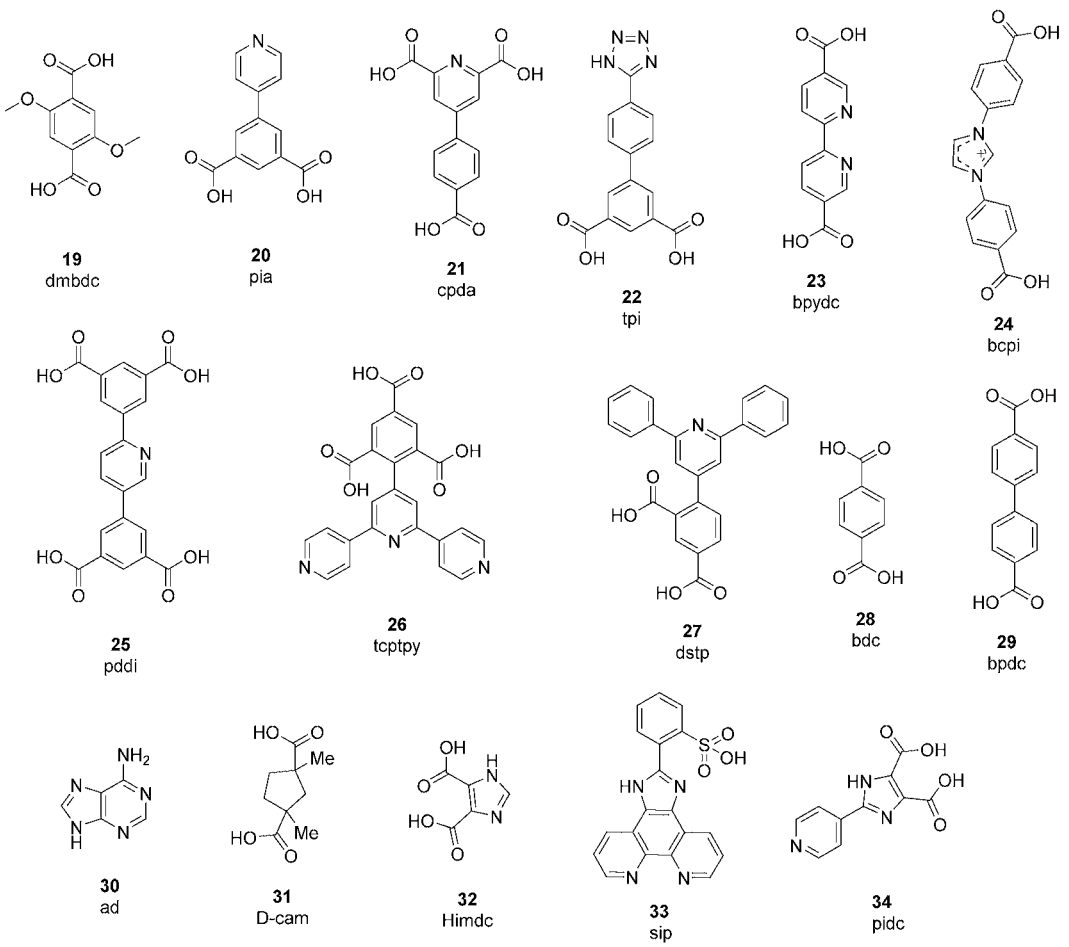

Figure 8. Overview of the N-rich antennae incorporated in metal–organic frameworks for temperature sensing.

dination sites. The $Tb_{0.995}Eu_{0.005}$@In(OH)(bpydc) showed temperature dependency in the region 283–333 K with a maximum temperature sensitivity of 4.47% K^{-1} at 333 K. Moreover, the reproducibility and repeatability of the material were tested and approved. The mechanism involves energy transfer from Tb^{3+} to Eu^{3+} and energy back transfer from the emitting level of Tb^{3+} to the excited triplet state of the bpydc ligand. The triplet excited state energy was however not determined. Furthermore, the research team analogously synthesized $Tb_{0.995}Eu_{0.005}$@MOF-253 (MOF-253 = Al(OH)(bpydc)) and $Tb_{0.995}Eu_{0.005}$@COMOC-4 (COMOC-4 = Ga(OH)(bpydc)) with temperature sensitivities of 2.54% K^{-1} and 1.97% K^{-1} respectively, in the same temperature region. This work proves the importance of the choice of the metal node, on top of the ligands and (the percentage of) lanthanide ions. Yan and co-workers further reported post-synthetic functionalization of the bpydc-UiO-67 MOF (Zr used as metal node) with chlorine salts of Eu^{3+} and Tb^{3+}, resulting in the nanocrystalline material $Tb_{0.005}Eu_{0.995}$@UiO-67-bpydc.[77] The sensor operates in the temperature region 100–300 K with a maximum temperature sensitivity of 0.5% K^{-1}. However, they claim to have the highest reported temperature sensitivity of 47.98% K^{-1}, overselling their results with a factor 100. Kaczmarek et al. used the MOF $[Tb_2(bpydc)_3(H_2O)_3]\cdot n$DMF as a platform and grafted β-diketonate complexes of Eu^{3+} onto the bipyridine linkers through post-synthetic functionalization.[78] The MOF selected in this work showed breathing behaviour in the structure. Removal of the DMF solvents would result in a structure transformation, and a nonporous material would be formed. Two sensors were developed by changing the percentage of added Eu^{3+}complexes, the sensor with 7.3% Eu^{3+} showed temperature dependency in the range 200–325 K with a maximum relative sensitivity of 1.33% K^{-1} (325 K), and the sensor with 3% Eu^{3+} is operational from 225–375 K with a maximal sensitivity of 2.59% K^{-1} (225 K). The lowest triplet energy excited state energy of bpydc is 21 505 cm^{-1}. They observe efficient energy transfer from the ligand to Tb^{3+}. Moreover, the same research group developed the rare Tb^{3+}/Sm^{3+} codoped MOF253, functionalized with different β-diketonate complexes (acac and tfac).[79] The material $Tb_{0.9}Sm_{0.1}$MOF253_acac showed temperature dependency in the region 250–410 K, with a maximum relative thermal sensitivity of 1.87% K^{-1} (410 K). $Tb_{0.95}Sm_{0.05}$MOF253_tfac is active as thermometer in the same temperature region, with a maximum of 13.72% K^{-1} (250 K). Wang et al. developed three MOF-based temperature sensors, operative from 40 to 300 K, with the ligand 1,3-bis(4-carboxyphenyl)imidazolium (bcpi) **24**: $Tb_{0.9}Eu_{0.1}$bcpi has a maximum relative sensitivity of 0.11% K^{-1} Table 2(300 K), $Tb_{0.8}Eu_{0.2}$L of 0.15% K^{-1} (300 K) and $Tb_{0.7}Eu_{0.3}$L of 0.17% K^{-1} (300 K).[80] In 2018, Qian and co-workers designed the MOF $Tb_{0.81}Eu_{0.19}$pddi (pddi: 5,5′-(pyridine-2,5-diyl)diisophthalic acid **25**) with a maximum sensitivity of 0.37% K^{-1} at 473 K, over the range 313–473 K.[81] The temperature range is clearly smaller and higher than the normal reported ranges. Furthermore, the MOF sensor showed good thermostability and spectral repeatability. The sensitivities correspond with a temperature resolution of 0.11–0.05 K. According to the authors, the accurate resolution suggest potential for the use in microelectronic diagnosis, since the accuracy is good enough to observe fluctuations in circuit chips. In 2020, Wang et al. developed a MOF with the ligand 4-(2,4,6-tricarboxylphenyl)-4,2′:6′,4′′-terpyridine (tcptpy) **26**, $Tb_{0.897}Eu_{0.103}$tcptpy.[82] The material is operative in the range 305–340 K and showed a high maximum sensitivity of 8.41% K^{-1} at 340 K. The calculated triplet excited state of the linker

Table 2. Overview of the different N-rich antennae used in MOF-based temperature sensors.

MOF	Temperature range [K]	S_m [% K^{-1}] at T_m [K]	Triplet level antenna [cm^{-1}]	Ref.
$Tb_{0.9931}Eu_{0.0069}$dmbdc **19**	50–200	1.15 (200)	23 306	[72]
$Tb_{0.9}Eu_{0.1}$pia **20**	100–300	3.53	26 455	[73]
$Tb_{0.957}Eu_{0.043}$cpda **21**	40–300	16 (300)	27 027	[74]
$Tb_{0.9122}Eu_{0.0878}$tpi **22**	75–250	4.9 (250)	21 505	[75]
$Tb_{0.995}Eu_{0.005}$@In(OH)(bpydc) **23**	283–333	4.47 (333)	21 505	[76]
$Tb_{0.995}Eu_{0.005}$@MOF-253 **23**	283–333	2.54	21 505	[76]
$Tb_{0.995}Eu_{0.005}$@COMOC-4 **23**	283–333	1.97	21 505	[76]
$Tb_{0.005}Eu_{0.995}$@UiO-67-bpydc **23**	100–300	0.5	21 505	[77]
TbMOF@7.3%Eu_tfac **23**	200–325	1.33 (325)	21 505	[78]
TbMOF@3%Eu_tfac **23**	225–375	2.59 (225)	21 505	[78]
$Tb_{0.9}Sm_{0.1}$MOF253_acac **23**	250–410	1.87 (410)	21 505	[79]
$Tb_{0.95}Sm_{0.05}$MOF253_tfac	250–410	13.72 (250)	21 505	[79]
$Tb_{0.9}Eu_{0.1}$bcpi **24**	40–300	0.11 (300)	ND	[80]
$Tb_{0.8}Eu_{0.2}$bcpi **24**	40–300	0.15 (300)	ND	[80]
$Tb_{0.7}Eu_{0.3}$ bcpi **24**	40–300	0.17 (300)	ND	[80]
$Tb_{0.81}Eu_{0.19}$pddi **25**	313–473	0.37 (473)	ND	[81]
$Tb_{0.897}Eu_{0.103}$tcptpy **26**	305–340	8.41 (340)	22 321	[82]
$[Tb_{0.98}Eu_{0.02}(OA)_{0.5}(dstp)]\cdot 3H_2O$ **27**	77–275	2.4 (275)	ND	[83]
$[Tb_{0.98}Eu_{0.02}(bdc)(dstp)]\cdot 3H_2O$ **27 28**	125–250	2.8 (225)	ND	[83]
Ad/$Tb_{0.999}Eu_{0.001}$/bpdc **29**	100–300	1.23	ND	[84]
$Eu_{0.7}Tb_{0.3}$(D-cam)$(Himdc)_2(H_2O)_2]_3$ **31 32**	100–450	0.11 (450)	ND	[85]
$[Eu:Tb(4:6)sip(glu)]_n\cdot 2nH_2O$ **33**	50–225	0.68	ND	[86]
$[Tb_{0.92}Eu_{0.08}pidc(ox)_{0.5}H_2O]\cdot 3H_2O$ **34**	303–473	0.6 (473)	ND	[88]

was 22 321 cm^{-1} and effective ligand-to-metal energy transfer was observed. The strategy of incorporating mixed ligands into a MOF was introduced by Wu et al., with the aim to investigate their influence on the temperature sensing properties. Wu and co-workers selected 2,4-(2,2′:6′,2″-terpyridin-4′-yl)-benzenedisulfonic acid (dstp **27**) as the first ligand and implemented an ancillary ligand as oxalic acid (OA) or 1,4-benzene dicarboxylic acid (bdc **28**).[83] The ancillary ligands enhance the thermal stability of the MOF, creating a thermally stable MOF up to 653 K and 788 K, respectively. They have successfully developed two types of highly thermal stable and sensitive thermometers $[Tb_{0.98}Eu_{0.02}(OA)_{0.5}(dstp)]\cdot 3H_2O$ and $[Tb_{0.98}Eu_{0.02}(bdc)(dstp)]\cdot 3H_2O$. The first sensor operates in the 77–275 K region with a maximum temperature sensitivity of 2.4% K^{-1} at 275 K, the second operates in the range of 125–250 K with 2.8% K^{-1} at 225 K. The typical temperature dependent mechanism was proposed; light-harvesting via the DSTP ligand, with a large π-conjugated system, and efficient energy transfer from Tb^{3+} to Eu^{3+}. The higher sensitivity of the bdc **28**-based MOF was attributed to a more efficient energy transfer from Tb^{3+} to Eu^{3+}. Furthermore, five other groups investigated the use of mixed ligands for temperature sensing. Yan et al. reported a MOF with biphenyl-4,4′-dicarboxylate (bpdc) **29** and adenine (ad) **30** Ad/$Tb_{0.999}Eu_{0.001}$/bpdc, resulting in a thermometer operational in the 100–300 K region with a relative sensitivity of 1.23% K^{-1}.[84] The thermal stability was however not reported. Du and co-workers developed a MOF with the linkers D-camphoric acid (D-cam) **31** and 4,5-imidazole dicarboxylic acid (Himdc) **32**, $Eu_{0.7}Tb_{0.3}$(D-cam)$(Himdc)_2(H_2O)_2]_3$.[85] The temperature sensor operates with a sensitivity of 0.11% K^{-1} at 450 K in the range of 100–450 K. The MOF shows high thermal stability, up to 690 K. Hu et al. designed a Eu/Tb (4:6) coordination polymer with the ligands 2-(2-sulfophenyl)-imidazol(4,5-f)(1,10)-phenanthroline (sip) **33** and glutaric acid.[86] The material showed good thermal stability, up to 700 K. The sensor operates in the region 50–225 K with a sensitivity of 0.68% K^{-1}. Zareba and co-workers investigated two CP consisting both of phenanthroline and 1,3,5-benzenetricarboxylic acid (1,3,5-btc), the first MOF contains 0.88% Eu and 22.87% Tb (1Eu23Tb) and the second MOF contains 1.74% Eu and 21.88% Tb (2Eu22Tb).[87] Both sensors are active in the physiological 293–393 K range, 1Eu23Tb shows a relative sensitivity of 2.37% K^{-1} and 2Eu22Tb of 2.71% K^{-1}. At last, Liu and co-workers investigated the MOF $[Tb_{0.92}Eu_{0.08}pidc(ox)_{0.5}H_2O]\cdot 3H_2O$ with the ligand 2-pyridin-4-yl-4,5-imidazoledicarboxylic acid (pidc) **34** and the ancillary ligand sodium oxalate (ox).[88] The sensor operates in the region 303–473 K, with a maximum sensitivity of 0.6% K^{-1} at 473 K. The MOF is thermally stable up to 673 K. The authors claim a temperature resolution of 0.012 K. This low value implies the use of a detector with a relative uncertainty in Δ ($\delta\Delta/\Delta$) of 0.0072%. The current sensitive detectors (as the photomultiplier tube used in the cited paper) show $\delta\Delta/\Delta$ of 0.02–0.03%, making the reported temperature resolution of 0.012 K doubtful.[9,81] A low temperature resolution suggests the MOF is accurate enough to monitor the temperature changes in pathological and normal cells. The cytotoxicity (via MTT assay, a colorimetric assay for measuring the activity of enzymes that are capable of reducing the dye compound MTT (3-(4,5-dimethylthiazol-2-yl)-2,5-diphenyltetrazolium bromide)) and biocompatibility (stability in phosphate-buffered saline solution for 24 h) of the MOF is therefore tested and approved.

Table 2 provides an overview on the discussed temperature sensors. The relative temperature sensitivity is influenced by multiple factors. First, the lanthanide ions present and the ratio of these lanthanides is decisive. A large excess of the terbium ions over europium or samarium ions provides the best result. Next, the triplet level of the N-rich antenna plays a role. The highest reported sensitivity for the N-rich MOFs corresponds to the ligand with the highest triplet level. Third, the influence of the other ligands present in the lanthanide complex determine the outcome. This can clearly be seen from the influence of the β-diketones tfac and acac in the Tb/Sm based MOF. To put this table in perspective, the highest reported relative temperature sensitivity in MOFs is 31% K^{-1} (4 K) in the temperature region 4–50 K, obtained in the mixed-metal MOF $Tb_{0.95}Eu_{0.05}HL$ (H_4L: 5-hydroxy-1,2,4-benzenetricarboxylic acid).[89] The triplet level of the ligand is estimated to be 26 600 cm^{-1}. The energy difference between the triplet state of the ligand and the Tb^{3+} emitting level ($^5D_4$, 20 500 cm^{-1}) is approximately 6100 cm^{-1}, the energy can thus be transferred without significant energy back transfer. The MOFs generally operate in a broad temperature region, focusing on the physiological and cryogenic range. Their application potential therefore covers for example biological thermometers and the aerospace industry and superconducting magnets.[90] Higher temperatures are often not reported due to the thermal instability of these materials.

N-Rich Antennae Incorporated in Periodic Mesoporous Organosilicas

The following category of materials that will be discussed is the periodic mesoporous organosilicas (PMOs). PMOs are prepared through polycondensation of silica containing organic linkers around a template, and after removal of the template, a well-ordered mesoporous structure remains. Incorporating linkers with binding sites for lanthanide complexes recently gained attention. In 2018, the first report on the DPA PMO for visible light temperature sensing appeared. Kaczmarek et al. synthesized a PMO starting from 5% *N*,*N*-bis(trimethoxysilylpropyl)-2,6-pyridine dicarboxamide (dpa) **35** (Figure 9) and 95% tetraethyl orthosilicate, and grafted different ratios of Tb^{3+}/Eu^{3+} and Tb^{3+}/Sm^{3+} chloride salts onto the material.[91] To enhance the luminescence, 1,10-phenanthroline was added as a co-ligand in the grafting process. The Tb^{3+}/Eu^{3+} grafted PMO nanoparticles showed temperature dependent behaviour in the region 260–460 K. $Eu_{0.25}Tb_{0.75}$DPA-PMO has a maximum relative sensitivity of 1.22% K^{-1} (440 K), $Eu_{0.50}Tb_{0.50}$DPA-PMO a maximum of 1.56% K^{-1} (360 K) and $Eu_{0.75}Tb_{0.25}$DPA-PMO a maximum of 1.45% K^{-1} (340 K). The authors observe energy transfer from Tb^{3+} to Eu^{3+}, suggesting that they graft closely together onto the PMO framework. As can be seen, a specific choice of the lanthanide ratio is important. The sensor $Sm_{0.95}Tb_{0.05}$DPA-PMO is operational in the region 280–460 K

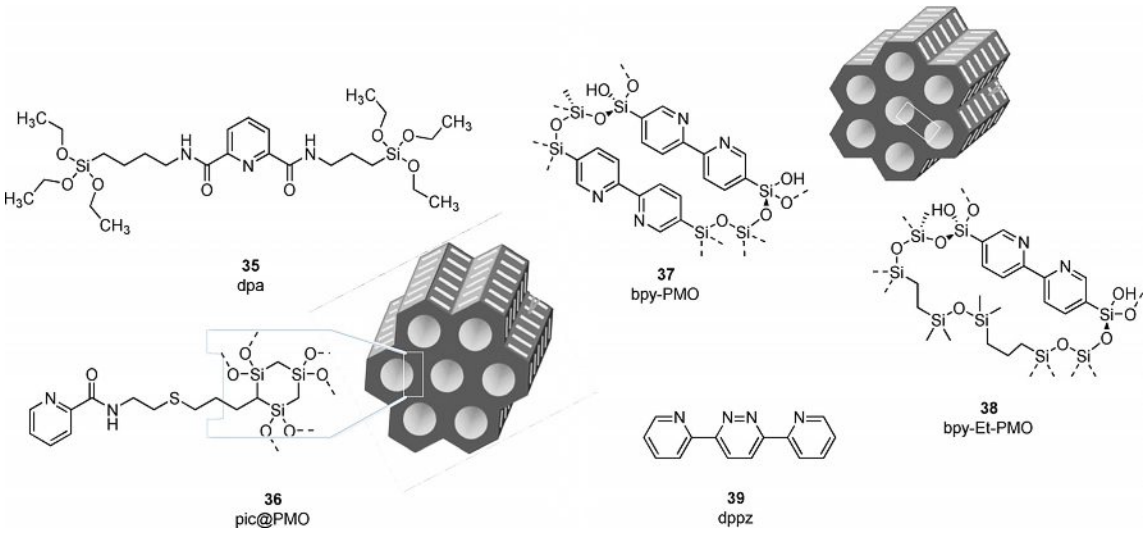

Figure 9. Reported lanthanide grafted PMO materials tested for temperature sensing.

with a maximum relative sensitivity of 2.38% K^{-1} (340 K). Energy transfer from Tb^{3+} to Sm^{3+} is observed based on the changing decay times over the temperature interval. Obtaining strong Sm^{3+} emission (especially at elevated temperature) is difficult, therefore, Tb^{3+}/Sm^{3+} based sensors are rare. All these sensors are operational in the broad physiological range, moreover PMOs are known for their high biocompatibility, making them attractive, potential biological nanothermometers.[42] In 2019, Jena, Kaczmarek and co-workers coupled picolinic acid onto a monoallyl ring PMO via thiol-ene click chemistry.[92] Afterwards, equal molar ratios of Eu^{3+} and Tb^{3+} ions were grafted onto the material resulting in $Eu_{0.5}Tb_{0.5}$@Pic@PMO **36**. The triplet level of the Pic@PMO was estimated around 25 252 cm^{-1}. The energy of the ligand is efficiently transferred from the ligand to the Tb^{3+} emitting level, and subsequent Tb-to-Eu energy transfer. This process proves close proximity of the lanthanide ions. The materials operates as a thermometer with a maximum relative sensitivity of 2.1078% K^{-1} (273 K) in the physiological region (270–373 K). In 2020, Inagaki, Van Der Voort and co-workers developed Dy-Dy and Tb-Sm based bipyridine PMOs.[93] They investigated pure 2,2′-bipyridine PMO (bpy-PMO **37**) and a bipyridine-ethane co-condensed PMO (bpy-Et-PMO **38**). Grafting of $Dy(acac)_3$ complexes onto bpy-PMO, resulted in a sensor operational in the temperature region 200–400 K with a maximum relative sensitivity of 2.85% K^{-1} (200 K). When $Dy(acac)_3$ complexes were grafted onto bpy-Et-PMO, a sensor with maximum sensitivity of 1.46% K^{-1} (300 K) in the region 200–400 K was obtained. With temperature increase, the higher energy level of Dy^{3+} ($^4I_{15/2}$) becomes populated and, hence, its emission intensity increases gradually, at the expense of the population of the lower state ($^4F_{9/2}$). A ratiometric temperature sensor is established from the changing intensity ratio of these peaks. Furthermore, the authors investigated the thermometer potential when grafting multiple ratios of Tb^{3+}/Sm^{3+} onto the different PMOs. The bpyPMOs showed temperature dependency in the region 253–333 K, $Sm_{0.9}Tb_{0.1}(acac)_3$bpy-PMO with a maximum relative sensitivity as high as 4.93% K^{-1} (253 K) and $Sm_{0.8}Tb_{0.2}(acac)_3$bpy-PMO a maximum of 4.82% K^{-1} (253 K). The sensors based on bpy-Et-PMO are operational in the region 253–373 K, $Sm_{0.9}Tb_{0.1}(acac)_3$bpy-Et-PMO shows a maximum sensitivity of 3.83% K^{-1} (323 K), $Sm_{0.8}Tb_{0.2}(acac)_3$bpy-Et-PMO a maximum of 3.72% K^{-1} (323 K). The sensors consisting of pure bipyridine linkers are better thermometers, furthermore, a higher amount of Sm^{3+} over Tb^{3+} is beneficial. The (grafted) PMO materials were tested for their toxicity towards fibroblastic cells of normal human dermal fibroblasts, showing a complete absence of toxicity. Furthermore, the materials were tested in water, forming stable colloidal suspensions, and showing very good thermometric properties. The investigated materials could therefore be promising candidates for biomedical temperature sensing, despite being excited and emitting in the visible region and not the NIR region, which is more favorable for biomedical temperature sensing due to deeper tissue penetration. They could be useful for example in the fundamental studies of the biological, biochemical and physiological processes happening in cells where visible light is suitable for use.

Furthermore, a mesoporous silica (this material is not a PMO since its synthesis is conducted in the presence of a silica source (TEOS)) decorated with dipyridyl-pyridazine (dppz) **39** ligands and grafted with 28% Eu^{3+} and 72% Tb^{3+} ions was investigated by Kaczmarek and co-workers as a temperature sensor.[94] The material showed a maximum relative sensitivity of 1.32% K^{-1} (260 K) over the range 10–360 K. The N-rich ligand dppz could also be used to prepare thermometers with NIR emitting lanthanides (Nd, Yb, Er).[95]

N-Rich Antennae Incorporated in Porous Organic Polymers

The fully organic counterpart of the metal–organic framework, covalent organic framework (COF), consist purely of covalently bonded, organic building blocks. Varying the building blocks results in a wide library of potential crystalline, porous 2D or

3D frameworks. COFs benefit from high thermal and chemical stability, making them ideal candidates for temperature sensing. In light of the application, organic π-systems are preferred over their saturated counterparts, since these system are more prone to electronic excitations (lower energy difference for a π–π* transition than for a σ–σ* transition). Until now (June 2020), only one report investigates the use of COFs in temperature sensing. Kaczmarek and co-workers started from the imine-linked TpBpy-COF, prepared from 1,3,5,-triformylphloroglucinol (Tp) **40** and 2,2′-bipyridine-5,5′-diamine (Bpy) **41** (Figure 11), and grafted different ratios of Eu^{3+}/Tb^{3+} and Dy^{3+} acetylacetone complexes onto the framework.[96] The Eu^{3+}/Tb^{3+} based temperature sensors all operate in the broad temperature region 10–360 K. Varying the ratio of Eu^{3+}/Tb^{3+} provided insight in the ideal composition. $Eu_{0.6}Tb_{0.4}$@TpBpyCOF shows a maximum relative sensitivity of 1.018% K^{-1} (160 K), $Eu_{0.8}Tb_{0.2}$@TpBpyCOF a maximum of 1.403% K^{-1} (160 K) and $Eu_{0.95}Tb_{0.5}$@TpBpyCOF a maximum of 1.342% K^{-1} (160 K). Remarkably, for all the sensors peculiar temperature dependent behaviour was observed; Tb^{3+} emission is namely not temperature dependent over the investigated range, as can be seen in Figure 10. This is related to the absence of energy back transfer from Tb^{3+} to the ligand, the energy of the lowest ligand triplet level (around 400 nm) is well above the $^5D_4$ acceptor level of Tb^{3+}. The excited Eu^{3+} levels (around 400 nm–25000 cm^{-1}) are however closer and allow metal-to-ligand back transfer, concomitantly decreasing the $^5D_0$ lifetime as temperature increases.[97] Furthermore, the phenomenon suggests no Tb^{3+} to Eu^{3+} energy transfer. This was studied in detail through monitoring the decay times over the temperature range, the decay time of Tb^{3+}indeed remained constant with increasing temperature. A second part of the manuscript focuses on $Dy(acac)_3$ grafted TpBpyCOF. The sensor operates in the region 280–440 K, with a maximum relative sensitivity of 0.942% K^{-1} (280 K). The temperature uncertainty is below 0.05 K, confirming the good thermometer performance. The potential of COFs in temperature sensing is tremendous. The use of the antennae could for example be further explored through the creation of more stable linkages and increasing the effectiveness of π-conjugation.[47] Furthermore, different temperature regions, compared to the reported MOFs, and subsequent different applications could be investigated.

So far, crystalline, porous materials were discussed as potential temperature sensor. Crystallinity was thought to have a crucial influence on the luminescent properties. The interactions between monomer units and adjacent layers are less understood in amorphous systems. Nevertheless, we found it interesting to investigate the potential of amorphous materials in temperature sensing. In 2020, Kaczmarek et al. were the first to explore an amorphous, porous organic polymer (POP) for temperature sensing. The starting materials are 6,6′-(2,2′-bipyridine-5,5′-diyl)bis(1,3,5-triazine-2,4-diamine) (bpyDAT) **42** and terephthalaldehyde **43** (Figure 11), creating an aminal connected framework. The framework is grafted with two different Eu^{3+}/Tb^{3+} ratios. $Tb_{0.5}Eu_{0.5}$@BpyDAT POP **44** is operative in the region 10–310 K, with a maximum sensitivity of 0.81% K^{-1} (160 K). $Tb_{0.66}Eu_{0.34}$@BpyDAT POP showed temperature dependency in the 10–310 K, with a maximum sensitivity of 1.00% K^{-1} (125 K). The temperature uncertainty is below 0.25 K for the region 60–310 K and the material revealed excellent repeatability of 98.5%. The peculiar temperature behavior, constant Tb^{3+} emission over the whole temperature range (as observed for the Eu^{3+}/Tb^{3+} grafted TpBpyCOF discussed above), is detected. The behavior is explained through the same observations. First, the absence of ligand-to-Tb^{3+} energy back transfer is confirmed, since the triplet excited state energy of the ligand (24040 cm^{-1}) lies well above the $^5D_0$ accepting level of Tb^{3+}. Second, electronic communication from Tb^{3+} to Eu^{3+} is limited as the conjugation in the material is interrupted at the aminal nodes, this is further proven by a constant decay time for Tb^{3+}. For future research, the investigation of fully conjugated frameworks is therefore recommended.

Conclusion and Perspectives

The market share of noncontact temperature sensors is expending due to fast technological and medical evolutions. Lanthanide-based temperature sensors are the ideal thermometer

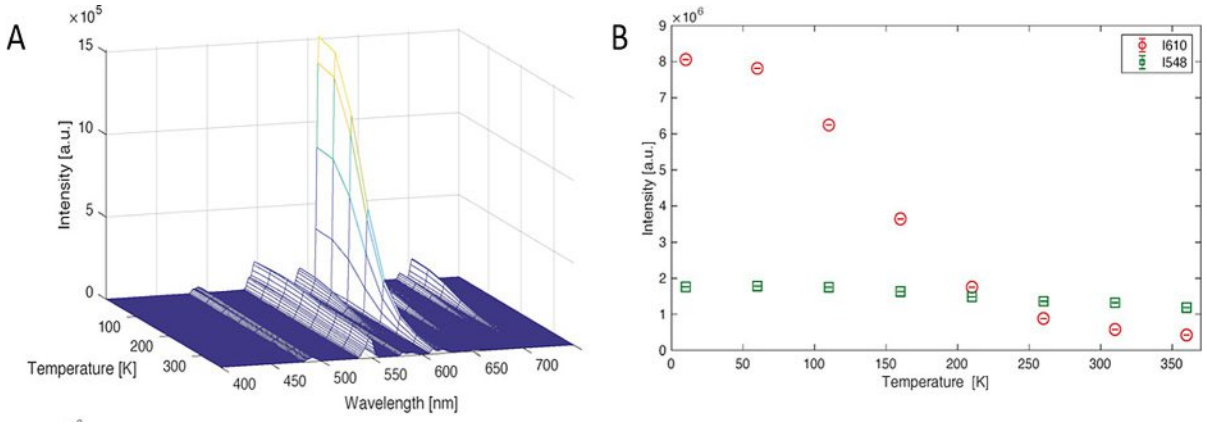

Figure 10. Plots for sample $Eu_{0.8}Tb_{0.2}$@TpBpyCOF. A shows the emission map recorded between 10–260 K and plot B the integrated-area values as a function of temperature. The green squares correlate to the 548 nm values, the red circles to the 610 nm values. The emission of Tb^{3+} (green squares) does not show temperature dependency. Reproduced with permission from Ref. [96]. Copyright 2020, Wiley-VCH.

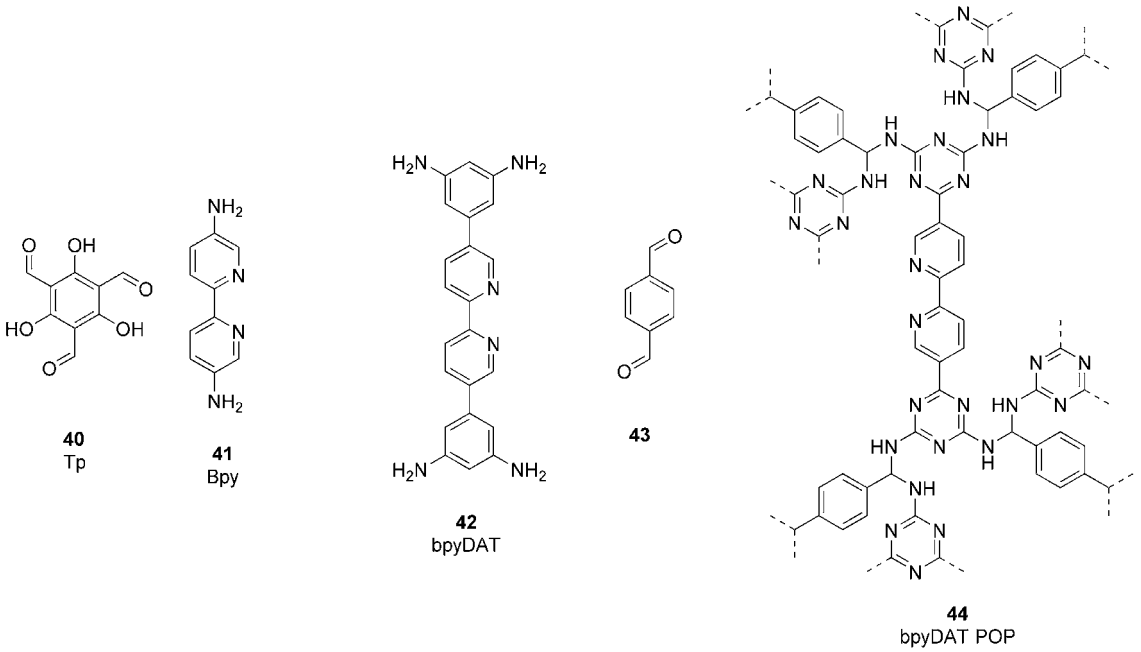

Figure 11. Building blocks of the reported COF and POP investigated for temperature sensing.

candidates as they benefit from high photostability, relatively long decay times and high quantum yields. To circumvent their low molar light absorption, the incorporation of a light-harvesting antenna is required. This Review presented the development of the N-rich lanthanide-based temperature sensors, emitting in the visible-light spectrum. The N-rich antenna enables first, the formation of a Lewis adduct, second, influences energy transfers through its triplet level and third, minimizes radiationless deactivation of the sensor. The N-rich ligands are incorporated in many different platforms. First, the molecular probes were discussed, containing a single trivalent lanthanide ion. Eu^{3+} is mostly reported and the corresponding sensors operate in the broad physiological range. The sensor based on Tb^{3+} is operational in a lower temperature range. Their application potential covers mainly temperature sensitive paints and intracellular temperature mapping, however, many systems have not been developed into applications. The path towards the final goal includes multiple obstacles (e.g. assessing bioavailability and toxicity), requiring an interdisciplinary approach. Moreover, the ratiometric temperature sensor is introduced, either as single- or dual-center, to cancel out influences from inhomogeneity in the material or the environment. Different N-rich platforms have been addressed.

This Review presents the investigation of N-rich antennae incorporated in polymers, MOFs, PMOs, and recently, in COFs and POPs. Overall, a very specific choice of lanthanide ratio provides the best result, testing and reporting of the multiple attempts are advised for a better understanding in the future. Generally, a higher amount of Tb^{3+} over Eu^{3+} was mostly reported. The antenna mainly determines the application potential of the ratiometric thermometer. Metal–organic frameworks are generally very useful in the cryogenic region, periodic mesoporous organosilica show temperature dependency in the physiological range and porous organic polymers are operative in the cryogenic to medium temperature range. Formulating conclusions over and in the different types of materials explored for temperature sensing, remains hard. The outcome is namely influenced by different parameters and comparison could only be decisive if only one parameter was changed. The investigation of different platforms opens up opportunities of the sensors in different temperature regions, and coherently, in different applications. A more fundamental growth is expected in the novel research field of COFs as temperature sensor, while the more established researched platforms as MOFs will elaborate the application potential as thermometer. To improve and accelerate the global result, more coherence in the reported characteristics over the different research groups worldwide (especially the accessible information for example, Tb^{3+}/Eu^{3+} ratios tested, triplet level antenna) is advised. The growth potential of lanthanide-based temperature sensors could also expand when the understanding on the energy transfer mechanisms is elaborated. As described in this Review, the recently explored material categories COFs and POPs show peculiar temperature behavior due to modified energy transfer mechanisms. Further investigation of other COFs and POPs would therefore be required to observe a possible trend in the reported peculiar behavior. Moreover, the synthesis of a single crystal COF could allow precise determination of the location of Tb^{3+} and Eu^{3+} ions in the framework. In this way, the distance between the different ion centers could be unraveled and further investigation of the proposed energy transfer mechanisms could be investigated. Gaining insight into the nature and main features of energy transfer mechanisms is essential to predict materials with low energy loss and high radiation efficiency. The research should therefore go beyond the experimental obtained results. However, it should be men-

tioned here that understanding and predicting energy transfer thermometry is far from a trivial task. Only recently, the first theoretical framework for ratiometric single ion luminescent thermometry has been laid.[98] We hope that further work on more complex to study energy transfer thermometry will also be reported soon. Some computational studies have been conducted for mononuclear and dinuclear lanthanide complexes of Eu^{3+} and Tb^{3+} ions.[99,100] However, MOFs, PMOs, COFs and POPs contain multiple ligands and lanthanide ions, therefore, the modelled energy transfers for a single complex must be extended towards the developed mixture of active centers in the framework. In this way, the combination of theoretical and experimental input could provide insights in the energy transfer mechanisms. Furthermore, computational studies allow more efficient and targeted experimental development of novel antennae. The energy gap between the lowest triplet level of the ligand and the emitting level of the lanthanide ion is key in determining the luminescence performance. Through computational studies, the excited states can be localized and the triplet level of novel antennae can be calculated, in this way, the influence of for example different substituents on the triplet level of different antennae are investigated. The experimental results of the performance of the temperature sensor therefore provide input for advanced modelling studies, creating a smart methodology for the future development of temperature sensors.

Acknowledgements

This work is supported by the Research Board of Ghent University (BOF) through a Concerted Research Action (mandate FVB) (GOA 010-17).

Conflict of interest

The authors declare no conflict of interest.

Keywords: covalent organic frameworks · lanthanides · sensors · temperature sensing

[1] K. E. L. Michalski, J. Kucharski, J. McGhee in *Temperature Measurement*, Wiley, West Sussex, **2002**, pp. 471 – 478.
[2] R. P. Benedict, *Fundamentals of Temperature, Pressure and Flow Measurements*, Wiley, New York, **1977**.
[3] P. R. N. Childs, J. R. Greenwood, C. A. Long, *Rev. Sci. Instrum.* **2000**, *71*, 2959 – 2978.
[4] A. H. K. K. Khalid, *Sensors* **2008**, *8*, 5673 – 5744.
[5] K. M. McCabe, M. Hernandez, *Pediatr. Res.* **2010**, *67*, 469 – 475.
[6] D. Jaque, F. Vetrone, *Nanoscale* **2012**, *4*, 4301 – 4326.
[7] S. Uchiyama, C. Gota, T. Tsuji, N. Inada, *Chem. Commun.* **2017**, *53*, 10976 – 10992.
[8] Temperate sensor market, global forecast to 2027 (by product type, output, end-user industry, and geography); SE 2914; Markets and Markets: **2020**.
[9] C. D. S. Brites, A. Millán, L. D. Carlos in *Handbook on the Physics and Chemistry of Rare Earths, Vol. 49* (Eds.:B. Jean-Claude, K. P. Vitalij), Elsevier, **2016**, pp. 339 – 427.
[10] R. A. Ferreira, C. D. S. Brites, C. M. Vicente, P. P. Lima, A. R. Bastos, P. G. Marques, M. Hiltunen, L. D. Carlos, P. S. André, *Laser Photonics Rev.* **2013**, *7*, 1027 – 1035.
[11] R. He, J. R. V. de Aldana, G. L. Pedrola, F. Chen, D. Jaque, *Opt. Express* **2016**, *24*, 16156 – 16166.
[12] C. Brites, P. Pereira, N. João, A. Millán, V. Amaral, F. Palacio, L. A. D. Carlos, *Front. Chem.* **2013**, *1*, 9.
[13] O. A. Savchuk, J. Carvajal, J. Massons, C. Cascales, M. Aguiló, F. Díaz, *Sens. Actuators A* **2016**, *250*, 87 – 95.
[14] R. G. Geitenbeek, A.-E. Nieuwelink, T. S. Jacobs, B. B. Salzmann, J. Goetze, A. Meijerink, B. M. Weckhuysen, *ACS Catal.* **2018**, *8*, 2397 – 2401.
[15] C. Abram, B. Fond, F. Beyrau, *Prog. Energy Combust. Sci.* **2018**, *64*, 93 – 156.
[16] T. Miyagawa, T. Fujie, Ferdinandus, T. T. Vo Doan, H. Sato, S. Takeoka, *ACS Appl. Mater. Interfaces* **2016**, *8*, 33377 – 33385.
[17] Ferdinandus, S. Arai, S. Takeoka, S. I. Ishiwata, M. Suzuki, H. Sato, *ACS Sens.* **2016**, *1*, 1222 – 1227.
[18] R. Piñol, C. D. S. Brites, N. J. Silva, L. D. Carlos, A. Millán in *Nanomaterials for Magnetic and Optical Hyperthermia Applications* (Eds.: R. M. Fratila, J. M. De La Fuente), Elsevier, **2019**, pp. 139 – 172.
[19] O. A. Savchuk, O. F. Silvestre, R. M. R. Adão, J. B. Nieder, *Sci. Rep.* **2019**, *9*, 7535.
[20] S. Mateos, J. Lifante, C. Li, E. C. Ximendes, Muñoz-T. Ortiz, J. Yao, M. de la Fuente-Fernández, Á. L. García Villalón, M. Granado, I. Zabala Gutierrez, *Small* **2020**, *16*, 1907171.
[21] H. D. Santos, E. C. Ximendes, Iglesias-M. d. C. de la Cruz, Chaves-I. Coira, B. del Rosal, C. Jacinto, L. Monge, Rubia-I. Rodríguez, D. Ortega, S. Mateos, *Adv. Funct. Mater.* **2018**, *28*, 1803924.
[22] C. D. Brites, P. P. Lima, N. J. Silva, A. Millán, V. S. Amaral, F. Palacio, L. D. Carlos, *Nanoscale* **2012**, *4*, 4799 – 4829.
[23] C. D. S. Brites, S. Balabhadra, L. D. Carlos, *Adv. Opt. Mater.* **2019**, *7*, 1801239.
[24] S. J. Cho, D. Maysinger, M. Jain, B. Röder, S. Hackbarth, F. M. Winnik, *Langmuir* **2007**, *23*, 1974 – 1980.
[25] A. Gnach, T. Lipinski, A. Bednarkiewicz, J. Rybka, J. A. Capobianco, *Chem. Soc. Rev.* **2015**, *44*, 1561 – 1584.
[26] J.-C. G. Bünzli, *Acc. Chem. Res.* **2006**, *39*, 53 – 61.
[27] J.-C. G. Bünzli, C. Piguet, *Chem. Soc. Rev.* **2005**, *34*, 1048 – 1077.
[28] P. C. Sahu, C. S. Nagar Venkataraman, in *Encyclopedia of Metalloproteins* (Eds.: R. H. Kretsinger, V. N. Uversky, E. A. Permyakov), Springer, New York, **2013**, pp. 5 – 11.
[29] L. D. Carlos, R. A. S. Ferreira, V. d. Z. Bermudez, S. J. L. Ribeiro, *Adv. Mater.* **2009**, *21*, 509 – 534.
[30] K. Binnemans, *Chem. Rev.* **2009**, *109*, 4283 – 4374.
[31] J.-C. G. Bünzli, *Coord. Chem. Rev.* **2015**, *293 – 294*, 19 – 47.
[32] Y. Hasegawa, Y. Kitagawa, *J. Mater. Chem. C* **2019**, *7*, 7494 – 7511.
[33] V. Tsaryuk, A. Vologzhanina, K. Zhuravlev, V. Kudryashova, *J. Fluorine Chem.* **2017**, *197*, 87 – 93.
[34] S. Katagiri, Y. Tsukahara, Y. Hasegawa, Y. Wada, *Bull. Chem. Soc. Jpn.* **2007**, *80*, 1492 – 1503.
[35] S. Weissman, *J. Chem. Phys.* **1942**, *10*, 214 – 217.
[36] M. Bhaumik, *J. Chem. Phys.* **1964**, *40*, 3711 – 3715.
[37] R. C. Ohlmann, R. G. Charles, *J. Chem. Phys.* **1964**, *40*, 3131 – 3133.
[38] S. Sato, A. Ishii, C. Yamada, J. Kim, C. Ho Song, A. Fujiwara, M. Takata, M. Hasegawa, *Polym. J.* **2015**, *47*, 195 – 200.
[39] G. E. Khalil, K. Lau, G. D. Phelan, B. Carlson, M. Gouterman, J. B. Callis, L. R. Dalton, *Rev. Sci. Instrum.* **2004**, *75*, 192 – 206.
[40] M. M. Ogle, A. D. Smith McWilliams, B. Jiang, A. A. Martí, *ChemPhotoChem* **2020**, *4*, 255-270.
[41] J. Rocha, C. D. Brites, L. D. Carlos, *Chem. Eur. J.* **2016**, *22*, 14782 – 14795.
[42] A. M. Kaczmarek, P. Van Der Voort, *Materials* **2020**, *13*, 566.
[43] Y. Zhang, S. Yuan, G. Day, X. Wang, X. Yang, H.-C. Zhou, *Coord. Chem. Rev.* **2018**, *354*, 28 – 45.
[44] W. P. Lustig, S. Mukherjee, N. D. Rudd, A. V. Desai, J. Li, S. K. Ghosh, *Chem. Soc. Rev.* **2017**, *46*, 3242 – 3285.
[45] Y. Cui, F. Zhu, B. Chen, G. Qian, *Chem. Commun.* **2015**, *51*, 7420 – 7431.
[46] Y. Cui, J. Zhang, H. He, G. Qian, *Chem. Soc. Rev.* **2018**, *47*, 5740 – 5785.
[47] W. K. Haug, E. M. Moscarello, E. R. Wolfson, P. L. McGrier, *Chem. Soc. Rev.* **2020**, *49*, 839 – 864.

[48] X.-d. Wang, O. S. Wolfbeis, R. J. Meier, *Chem. Soc. Rev.* **2013**, *42*, 7834 – 7869.
[49] S. M. Borisov, O. S. Wolfbeis, *Anal. Chem.* **2006**, *78*, 5094 – 5101.
[50] B. Zelelow, G. E. Khalil, G. Phelan, B. Carlson, M. Gouterman, J. B. Callis, L. R. Dalton, *Sens. Actuators B* **2003**, *96*, 304 – 314.
[51] M. Mitsuishi, S. Kikuchi, T. Miyashita, Y. Amao, *J. Mater. Chem.* **2003**, *13*, 2875 – 2879.
[52] M. I. J. Stich, S. Nagl, O. S. Wolfbeis, U. Henne, M. Schaeferling, *Adv. Funct. Mater.* **2008**, *18*, 1399 – 1406.
[53] J. Yu, L. Sun, H. Peng, M. I. J. Stich, *J. Mater. Chem.* **2010**, *20*, 6975 – 6981.
[54] D. V. Lapaev, V. G. Nikiforov, V. S. Lobkov, A. A. Knyazev, R. M. Ziyatdinova, Y. G. Galyametdinov, *J. Mater. Chem. C* **2020**, *8*, 6273 – 6280.
[55] D. V. Lapaev, V. G. Nikiforov, V. S. Lobkov, A. A. Knyazev, Y. G. Galyametdinov, *Opt. Mater.* **2018**, *75*, 787 – 795.
[56] A. A. Knyazev, A. S. Krupin, E. Y. Molostova, K. A. Romanova, Y. G. Galyametdinov, *Inorg. Chem.* **2015**, *54*, 8987 – 8993.
[57] P. Kolodner, J. A. Tyson, *Appl. Phys. Lett.* **1983**, *42*, 117 – 119.
[58] Y. Hasegawa, K. Murakoshi, Y. Wada, S. Yanagida, J.-H. Kim, N. Nakashima, T. Yamanaka, *Chem. Phys. Lett.* **1996**, *248*, 8 – 12.
[59] M. T. Berry, P. S. May, H. Xu, *J. Phys. Chem.* **1996**, *100*, 9216 – 9222.
[60] D. V. Lapaev, V. G. Nikiforov, V. S. Lobkov, A. A. Knyazev, Y. G. Galyametdinov, *J. Mater. Chem. C* **2018**, *6*, 9475 – 9481.
[61] A. A. Kitos, D. A. Gálico, R. Castañeda, J. S. Ovens, M. Murugesu, J. L. Brusso, *Inorg. Chem.* **2020**, *59*, 11061 – 11070.
[62] X.-d. Wang, X.-h. Song, C. – *y.* He, C. J. Yang, G. Chen, X. Chen, *Anal. Chem.* **2011**, 83, 2434 – 2437.
[63] S. Lu, J. Sun, Y. Wang, W. Yu, M. Sun, S. Cui, *J. Rare Earths* **2018**, *36*, 669 – 674.
[64] S. Swavey, J. A. Krause, D. Collins, D. D'Cunha, A. Fratini, *Polyhedron* **2008**, *27*, 1061 – 1069.
[65] D. A. Gálico, R. Marin, G. Brunet, D. Errulat, E. Hemmer, F. A. Sigoli, J. O. Moilanen, M. Murugesu, *Chem. Eur. J.* **2019**, *25*, 14625 – 14637.
[66] X.-Q. Guo, L.-P. Zhou, L.-X. Cai, Q.-F. Sun, *Chem. Eur. J.* **2018**, *24*, 6936 – 6940.
[67] G. Bao, K.-L. Wong, D. Jin, P. A. Tanner, *Light: Sci. Appl.* **2018**, *7*, 96.
[68] D. Yang, D. Liu, C. Tian, S. Wang, H. Li, *J. Colloid Interface Sci.* **2018**, *519*, 11 – 17.
[69] X. Zhou, H. Wang, S. Jiang, G. Xiang, X. Tang, X. Luo, L. Li, X. Zhou, *Inorg. Chem.* **2019**, *58*, 3780 – 3788.
[70] F. Vanden Bussche, A. M. Kaczmarek, J. Schmidt, C. V. Stevens, P. Van Der Voort, *J. Mater. Chem. C* **2019**, *7*, 10972 – 10980.
[71] W. Liu, C. Chen, X. Huang, E. Xie, W. Liu, *Chem. Eur. J.* **2019**, *25*, 10054 – 10058.
[72] Y. Cui, H. Xu, Y. Yue, Z. Guo, J. Yu, Z. Chen, J. Gao, Y. Yang, G. Qian, B. Chen, *J. Am. Chem. Soc.* **2012**, *134*, 3979 – 3982.
[73] X. Rao, T. Song, J. Gao, Y. Cui, Y. Yang, C. Wu, B. Chen, G. Qian, *J. Am. Chem. Soc.* **2013**, *135*, 15559 – 15564.
[74] Y. Cui, W. Zou, R. Song, J. Yu, W. Zhang, Y. Yang, G. Qian, *Chem. Commun.* **2014**, *50*, 719 – 721.
[75] L.-L. Wu, J. Zhao, H. Wang, J. Wang, *CrystEngComm* **2016**, *18*, 4268 – 4271.
[76] Y. Zhou, B. Yan, F. Lei, *Chem. Commun.* **2014**, *50*, 15235 – 15238.
[77] Y. Zhou, B. Yan, *Nanoscale* **2015**, *7*, 4063 – 4069.
[78] A. M. Kaczmarek, Y.-Y. Liu, C. Wang, B. Laforce, L. Vincze, P. Van Der Voort, R. Van Deun, *Dalton Trans.* **2017**, *46*, 12717 – 12723.
[79] A. M. Kaczmarek, Y.-Y. Liu, C. Wang, B. Laforce, L. Vincze, P. Van Der Voort, K. Van Hecke, R. Van Deun, *Adv. Funct. Mater.* **2017**, *27*, 1700258.
[80] S.-N. Zhao, L.-J. Li, X.-Z. Song, M. Zhu, Z.-M. Hao, X. Meng, L.-L. Wu, J. Feng, S.-Y. Song, C. Wang, H.-J. Zhang, *Adv. Funct. Mater.* **2015**, *25*, 1463 – 1469.
[81] D. Zhao, H. Wang, G. Qian, *CrystEngComm* **2018**, *20*, 7395 – 7400.
[82] X. Feng, Y. Shang, H. Zhang, X. Liu, X. Wang, N. Chen, L. Wang, Z. Li, *Dalton Trans.* **2020**, *49*, 4741 – 4750.
[83] Y. Wei, R. Sa, Q. Li, K. Wu, *Dalton Trans.* **2015**, *44*, 3067 – 3074.
[84] X. Shen, Y. Lu, B. Yan, *Eur. J. Inorg. Chem.* **2015**, 916 – 919.
[85] Y.-H. Han, C.-B. Tian, Q.-H. Li, S.-W. Du, *J. Mater. Chem. C* **2014**, *2*, 8065 – 8070.
[86] R. An, H. Zhao, H.-M. Hu, X. Wang, M.-L. Yang, G. Xue, *Inorg. Chem.* **2016**, *55*, 871 – 876.
[87] J. K. Zaręba, M. Nyk, J. Janczak, M. Samoć, *ACS Appl. Mater. Interfaces* **2019**, *11*, 10435 – 10441.
[88] Y. Yang, H. Huang, Y. Wang, F. Qiu, Y. Feng, X. Song, X. Tang, G. Zhang, W. Liu, *Dalton Trans.* **2018**, *47*, 13384 – 13390.
[89] X. Liu, S. Akerboom, M. D. Jong, I. Mutikainen, S. Tanase, A. Meijerink, E. Bouwman, *Inorg. Chem.* **2015**, *54*, 11323 – 11329.
[90] M. Quintanilla, L. M. Liz-Marzán, *Nano Today* **2018**, *19*, 126 – 145.
[91] A. M. Kaczmarek, R. Van Deun, P. Van Der Voort, *J. Mater. Chem. C* **2019**, *7*, 4222 – 4229.
[92] L. Bourda, H. S. Jena, R. Van Deun, A. M. Kaczmarek, P. Van Der Voort, *J. Mater. Chem. A* **2019**, *7*, 14060 – 14069.
[93] A. M. Kaczmarek, Y. Maegawa, A. Abalymov, A. G. Skirtach, S. Inagaki, P. Van Der Voort, *ACS Appl. Mater. Interfaces* **2020**, *12*, 13540 – 13550.
[94] A. M. Kaczmarek, D. Esquivel, B. Laforce, L. Vincze, P. Van Der Voort, F. J. Romero-Salguero, R. Van Deun, *Luminescence* **2018**, *33*, 567 – 573.
[95] A. M. Kaczmarek, D. Esquivel, J. Ouwehand, P. Van Der Voort, F. J. Romero-Salguero, R. Van Deun, *Dalton Trans.* **2017**, *46*, 7878 – 7887.
[96] A. M. Kaczmarek, Y.-Y. Liu, M. K. Kaczmarek, H. Liu, F. Artizzu, L. D. Carlos, P. Van Der Voort, *Angew. Chem. Int. Ed.* **2020**, *59*, 1932 – 1940; *Angew. Chem.* **2020**, *132*, 1948 – 1956.
[97] G. H. Dieke, H. M. Crosswhite, H. Crosswhite, *Spectra and energy levels of rare earth ions in crystals*, Interscience Publishers, New York, **1968**.
[98] M. Suta, A. Meijerink, *Adv. Theory Simul.* **2020**, *3*, 2000176.
[99] K. A. Romanova, A. Y. Freidzon, A. A. Bagaturyants, Y. G. Galyametdinov, *J. Phys. Chem. A* **2014**, *118*, 11244 – 11252.
[100] Z. Yu, L. Shen, D. Li, E. Y. B. Pun, X. Zhao, H. Lin, *Sci. Rep.* **2020**, *10*, 926.

Manuscript received: January 2, 2021
Accepted manuscript online: February 4, 2021
Version of record online: March 16, 2021